Electronic Supplementary Information (ESI)

for

Experimental and theoretical insights into two tri- and tetranuclear Dy^{III} SMMs reveal the unusual superiority of triangular dodecahedral Dy^{III} over square antiprismatic Dy^{III} as an SIM centre

Abhishek Pramanik,[a,b] Shuvankar Mandal,[a,b] Parismita Borgohain,[c] Daniel O. T. A. Martins,[d] Hazel A. Sparkes,[e] Floriana Tuna,[d] Saurabh Kumar Singh[c]* and Sasankasekhar Mohanta[a]*

[a]Department of Chemistry, University of Calcutta, 92 A. P. C. Road, Kolkata 700 009, India, E-mail: sm_cu_chem@yahoo.co.in.
[b]Equal Contribution.
[c]Department of Chemistry, Indian Institute of Technology Hyderabad, Kandi-502284, Sangareddy, Telangana, India. E-mail: sksingh@chy.iith.ac.in
[d]National EPR Facility, Photon Science Institute, University of Manchester Oxford Road, Manchester, M13 9PL, United Kingdom
[e]School of Chemistry, University of Bristol, Cantock's Close, Bristol, BS8 1TS, UK

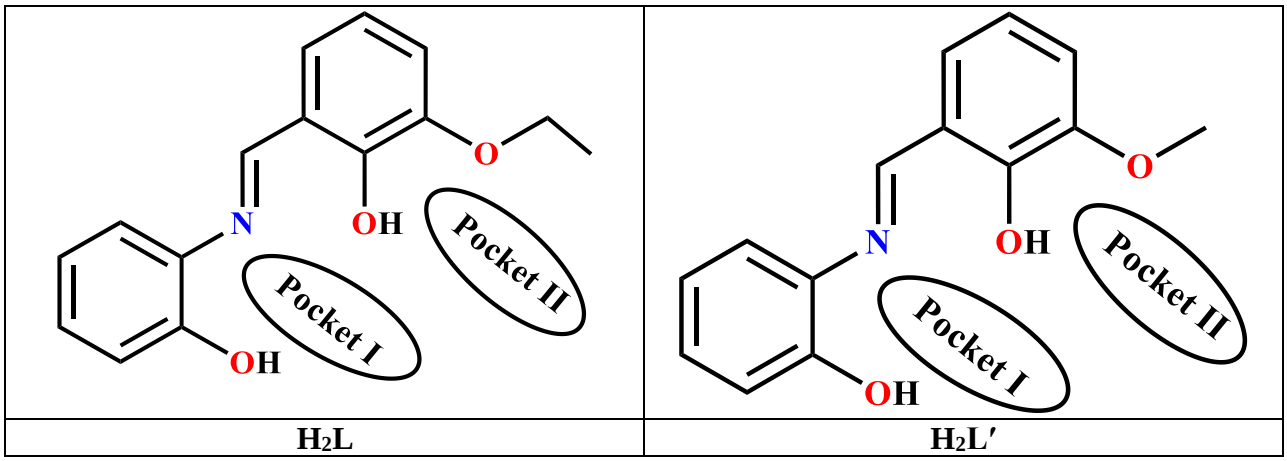

H_2L	H_2L'

Chart S1. Chemical structures of H_2L [2-(2-hydroxy-3-ethoxybenzylideneamino)phenol] and H_2L' [2-(2-hydroxy-3-methoxybenzylideneamino)phenol], showingtwo types of Pocket (I and II).

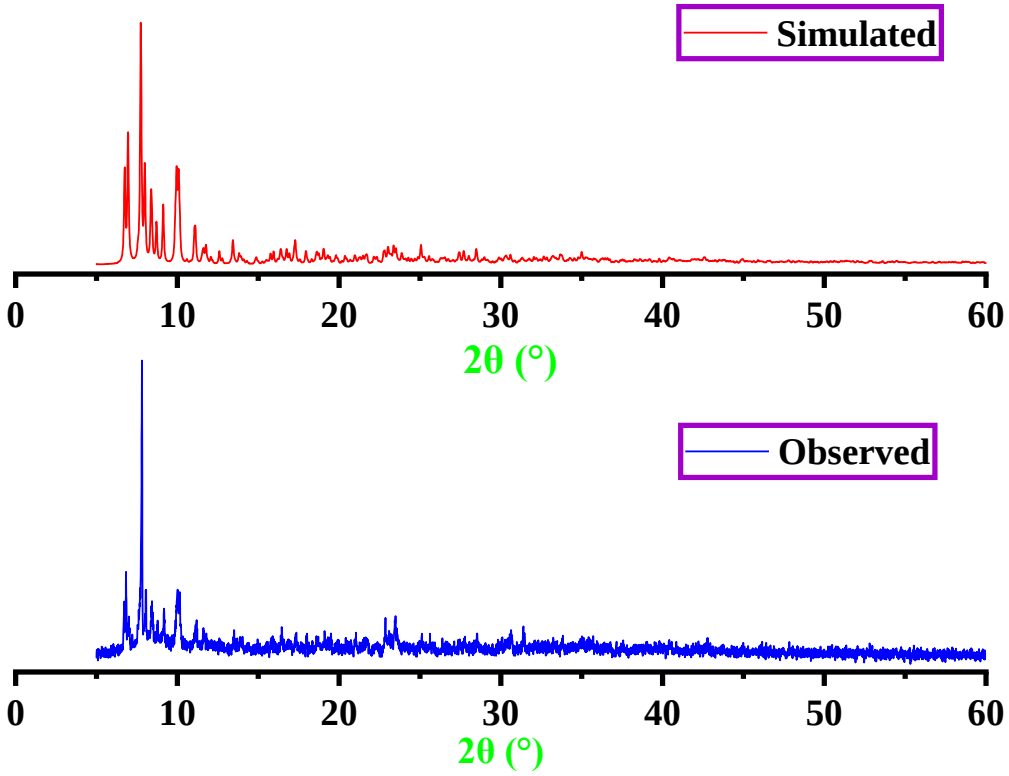

Fig. S1. Experimental (blue) and theoretical (red) powder X-ray diffraction (PXRD) profiles of $(Et_3NH)_2[Dy^{III}_3L_4(NO_3)_2]NO_3 \cdot 0.6Et_2O$ (**1**).

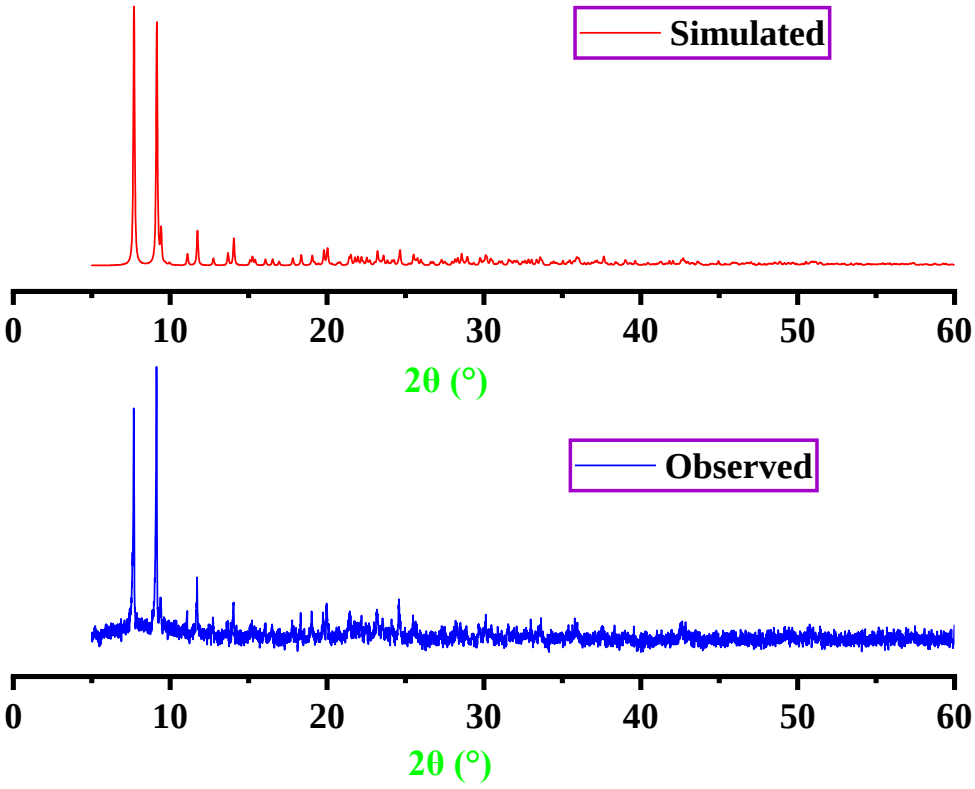

Fig. S2. Experimental (blue) and theoretical (red) powder X-ray diffraction (PXRD) profiles of $[Dy^{III}_4L_4(\mu_3\text{-}OH)_2(NO_3)_2(dmf)_2]$ (**2**).

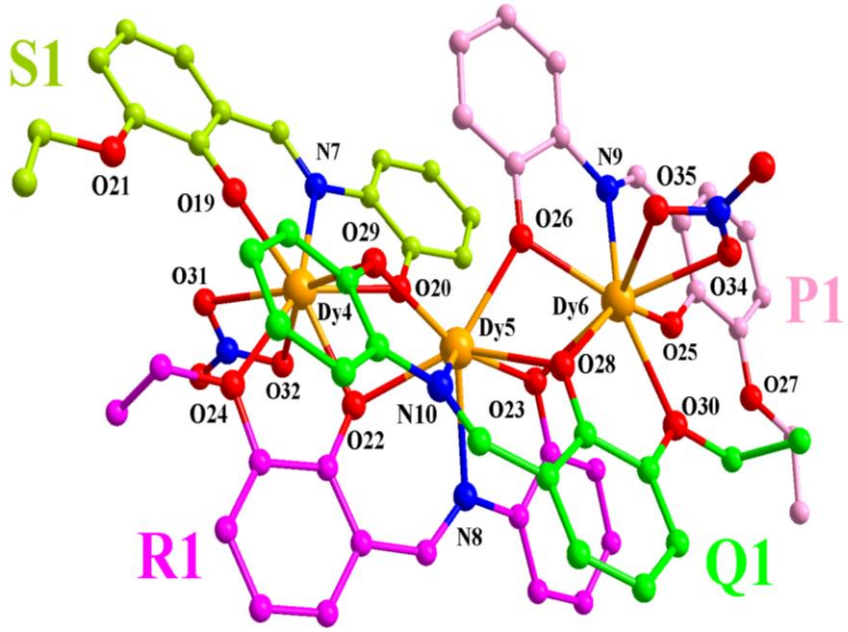

Fig. S3. Crystal structure of $[Dy^{III}_3L_4(NO_3)_2]^-$ anion in Unit II of $(Et_3NH)_2[Dy^{III}_3L_4(NO_3)_2]NO_3\cdot 0.6Et_2O$ (**1**). Hydrogen atoms are omitted for clarity.

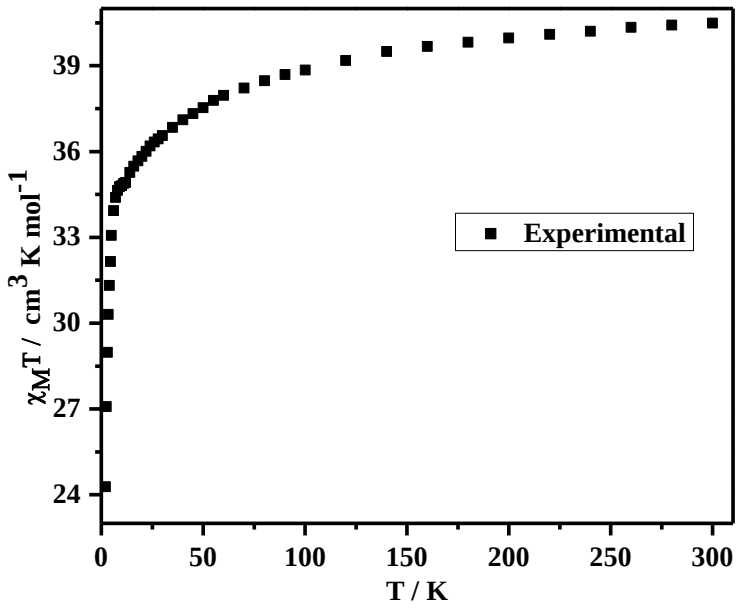

Fig. S4. Temperature dependence of the magnetic susceptibility in $\chi_M T$ vs T for $(Et_3NH)_2[Dy^{III}_3L_4(NO_3)_2]NO_3 \cdot 0.6Et_2O$ (**1**).

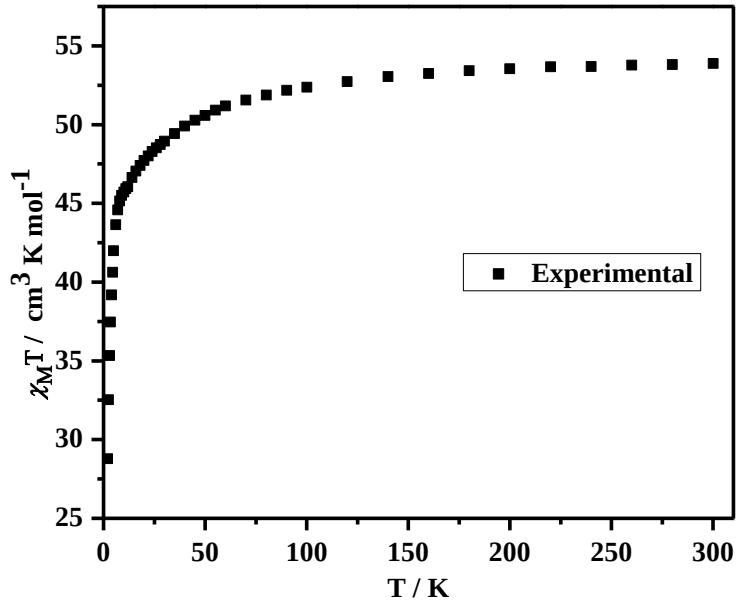

Fig. S5. Temperature dependence of the magnetic susceptibility in $\chi_M T$ vs T for $[Dy^{III}_4L_4(\mu_3\text{-}OH)_2(NO_3)_2(dmf)_2]$ **(2)**.

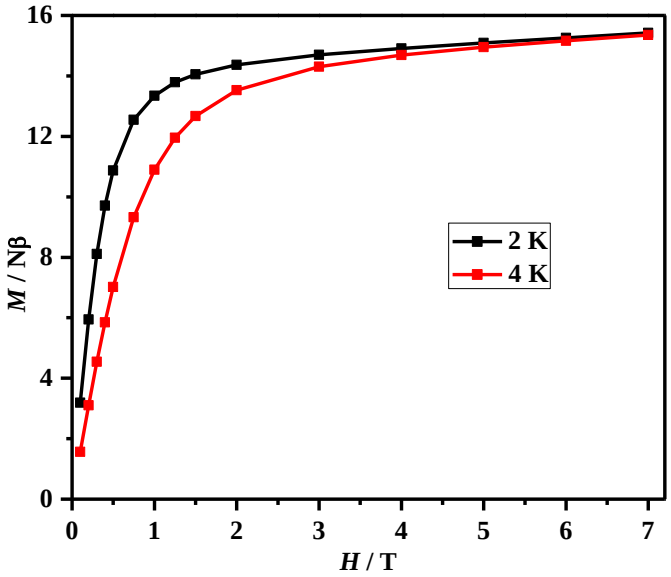

Fig. S6. Magnetization of $(Et_3NH)_2[Dy^{III}_3L_4(NO_3)_2]NO_3 \cdot 0.6Et_2O$ (**1**) in *M* vs *H*. The solid lines are guidelines for eyes.

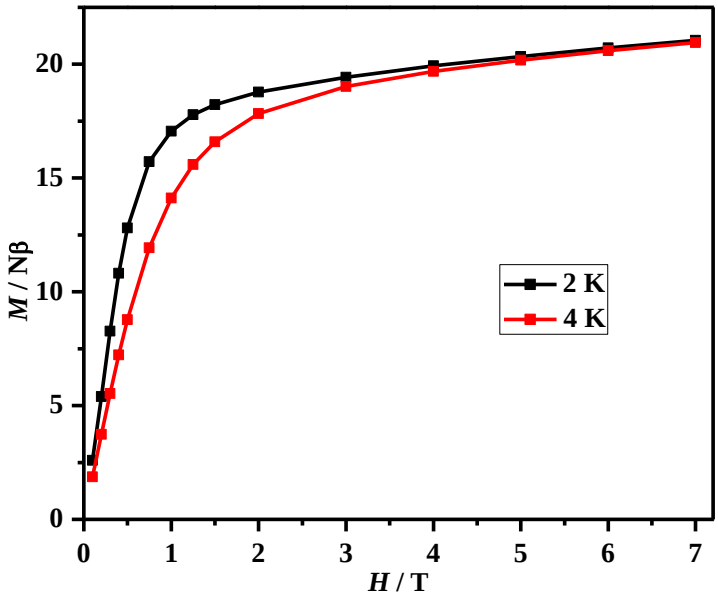

Fig. S7. Magnetization of $[Dy^{III}_4L_4(\mu_3\text{-}OH)_2(NO_3)_2(dmf)_2]$ **(2)** in *M* vs *H*. The solid lines are guidelines for eyes.

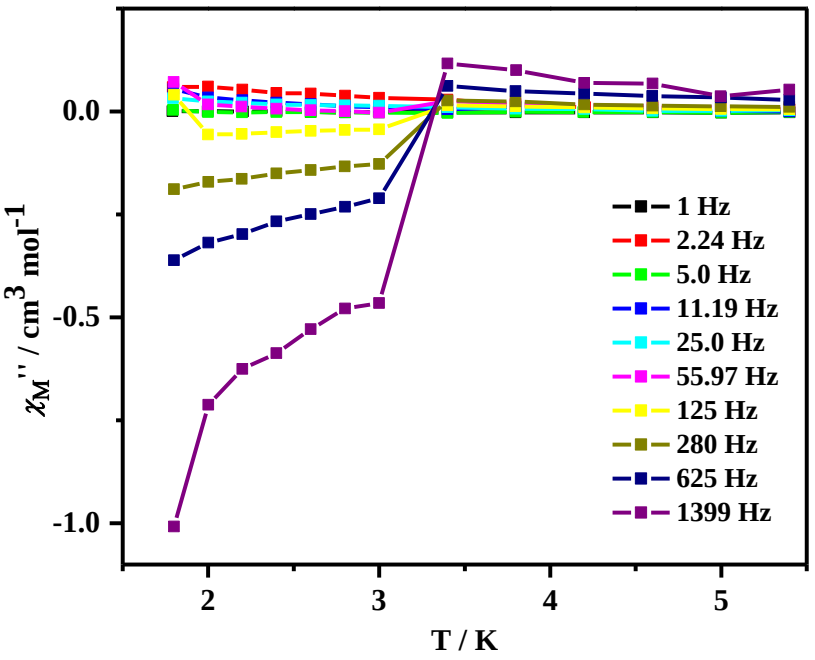

Fig. S8. Plots of the out-of-phase signal vs *T* at selected temperatures at different frequencies for $(Et_3NH)_2[Dy^{III}_3L_4(NO_3)_2]NO_3\cdot 0.6Et_2O$ (**1**) under zero dc field. The solid lines are guidelines for eyes.

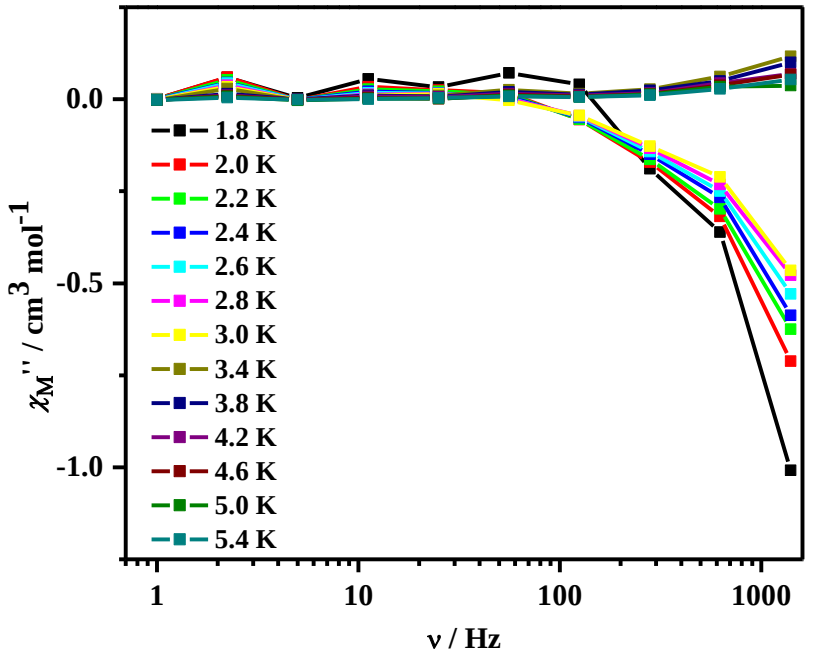

Fig. S9. Plots of the out-of-phase signal vs ν at selected temperatures for $(Et_3NH)_2[Dy^{III}_3L_4(NO_3)_2]NO_3\cdot 0.6Et_2O$ (**1**) under zero dc field. The solid lines are guidelines for eyes.

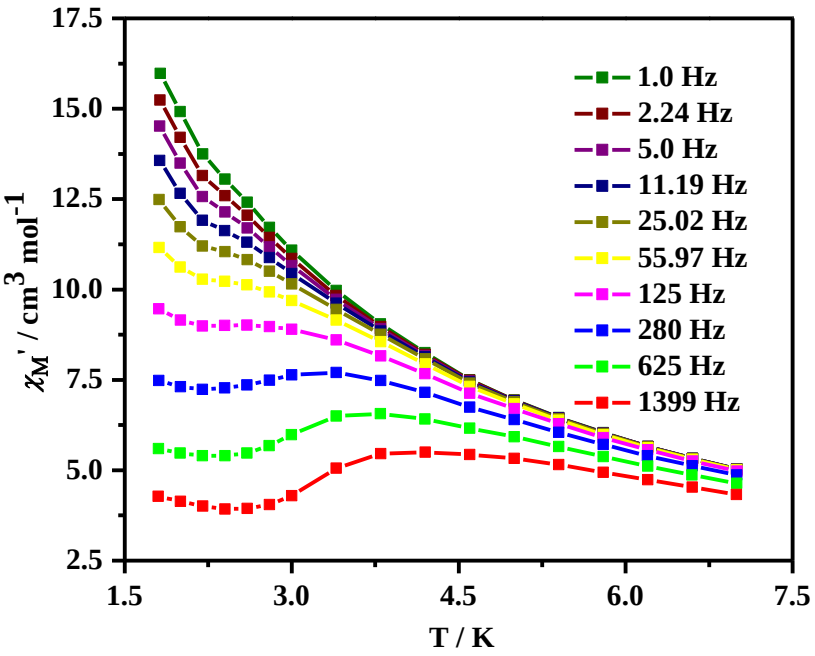

Fig. S10. Plots of the in-phase signal vs temperature at selected frequencies for $(Et_3NH)_2[Dy^{III}_3L_4(NO_3)_2]NO_3 \cdot 0.6Et_2O$ (**1**) at 1000 Oe. The solid lines are guidelines for eyes.

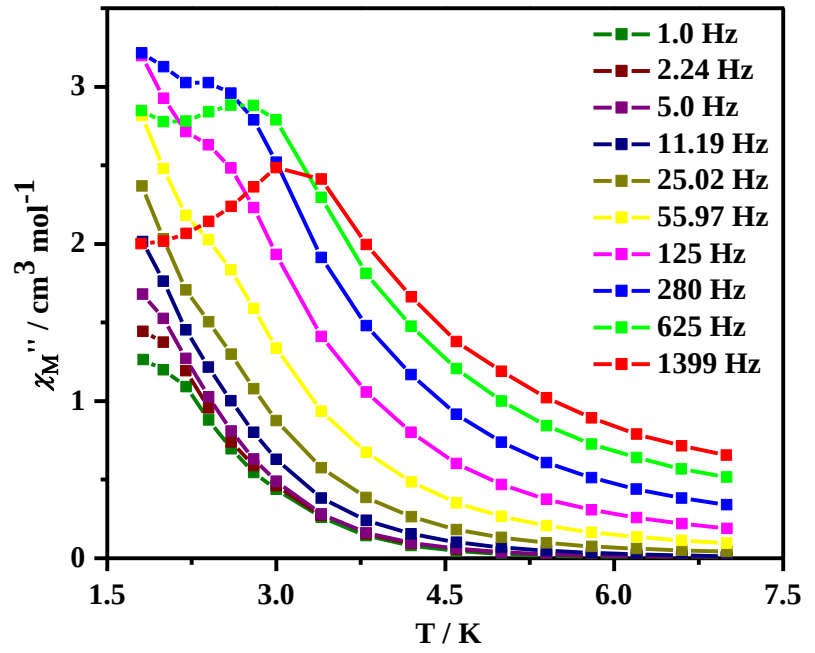

Fig. S11. Plots of the out-of-phase signal vs temperature at selected frequencies for $(Et_3NH)_2[Dy^{III}_3L_4(NO_3)_2]NO_3 \cdot 0.6Et_2O$ (**1**) at 1000 Oe. The solid lines are guidelines for eyes.

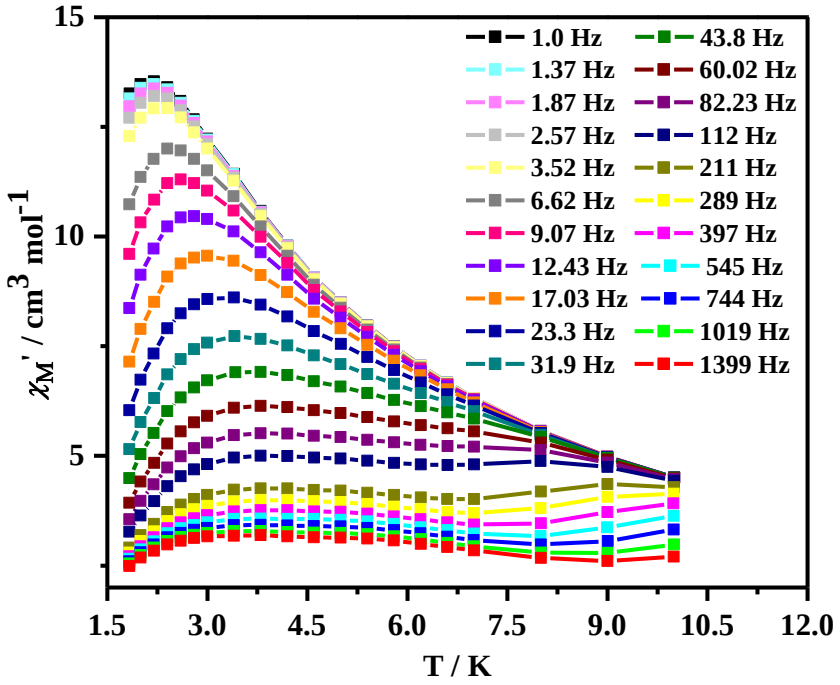

Fig. S12. Plots of the in-phase signal vs temperature at selected frequencies for [$Dy^{III}_4L_4(\mu_3\text{-}OH)_2(NO_3)_2(dmf)_2$] **(2)**. The solid lines are guidelines for eyes.

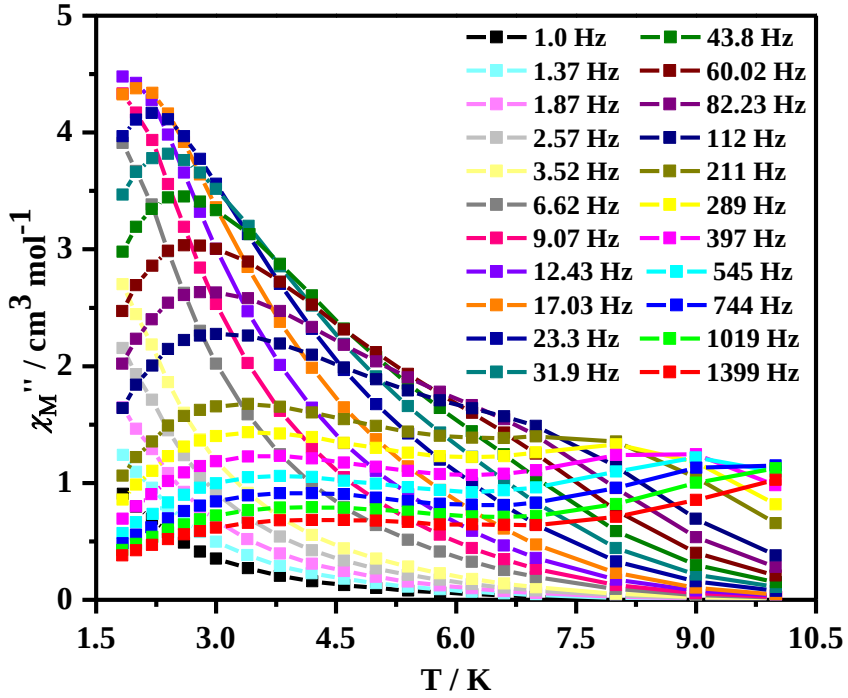

Fig. S13. Plots of the out-of-phase signal vs temperature at selected frequencies for [$Dy^{III}_4L_4(\mu_3\text{-}OH)_2(NO_3)_2(dmf)_2$] **(2)**. The solid lines are guidelines for eyes.

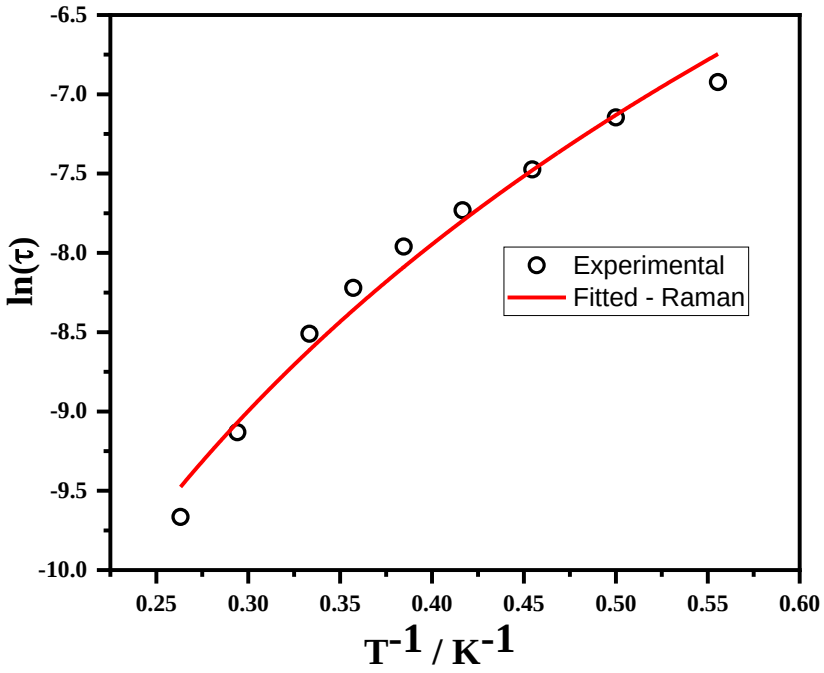

Fig. S14. Plot of the natural logarithm of the relaxation time vs the reciprocal temperature for $(Et_3NH)_2[Dy^{III}_3L_4(NO_3)_2]NO_3{\cdot}0.6Et_2O$ (**1**). Solid line corresponds to the best fit using Raman process.

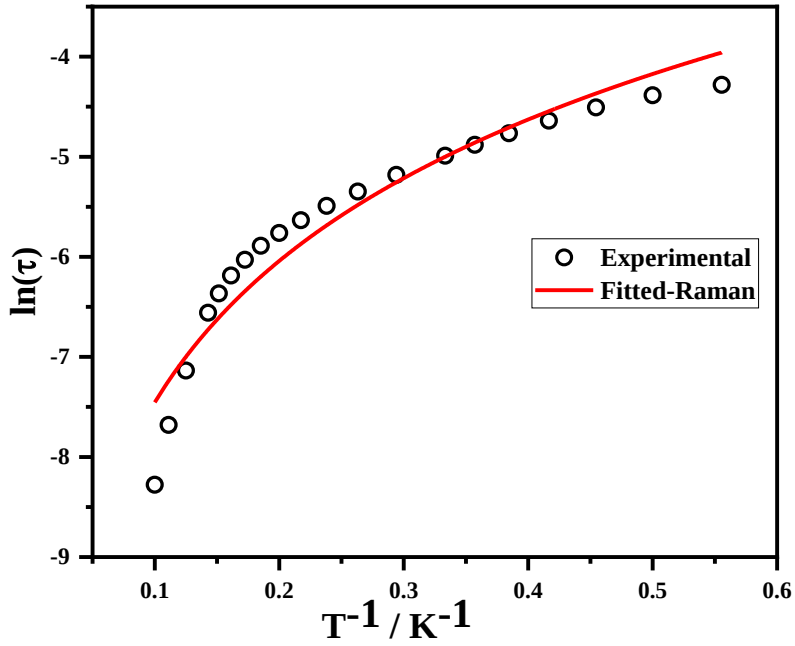

Fig. S15. Plot of the natural logarithm of the relaxation time vs the reciprocal temperature for $[Dy^{III}_4L_4(\mu_3\text{-}OH)_2(NO_3)_2(dmf)_2]$ **(2)**. Solid line corresponds to the best fit using Raman process.

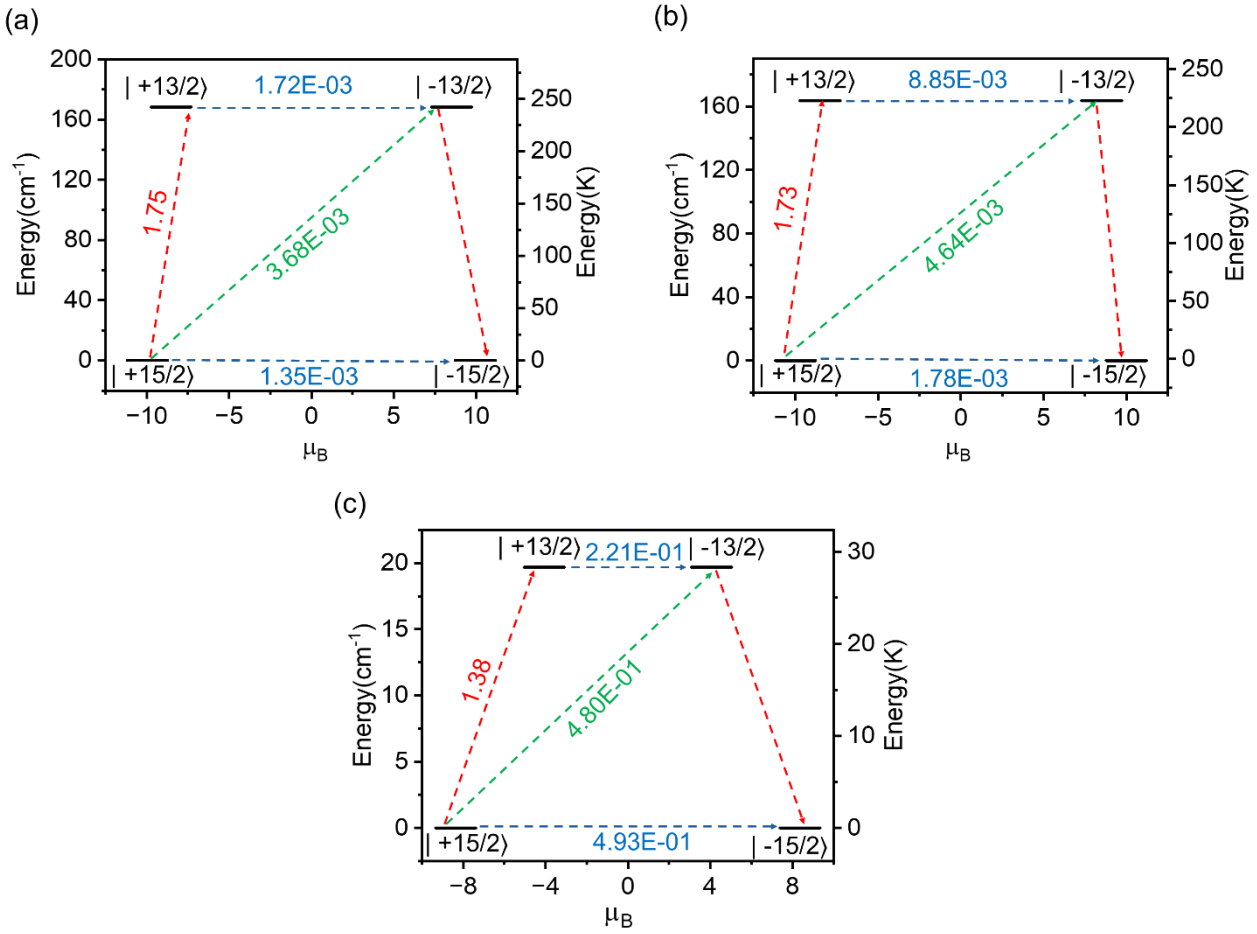

Fig. S16. SINGLE_ANISO computed *ab initio* blockade barrier for (a) **1**Dy@1, (b) **1**Dy@3, and (c) **1**Dy@2 centres of complex **1**. The black horizontal bars indicate the KDs as a magnetic moments function. The blue, red, and green arrows represent the possible QTM/TA-QTM, Orbach, and Raman relaxation pathways.

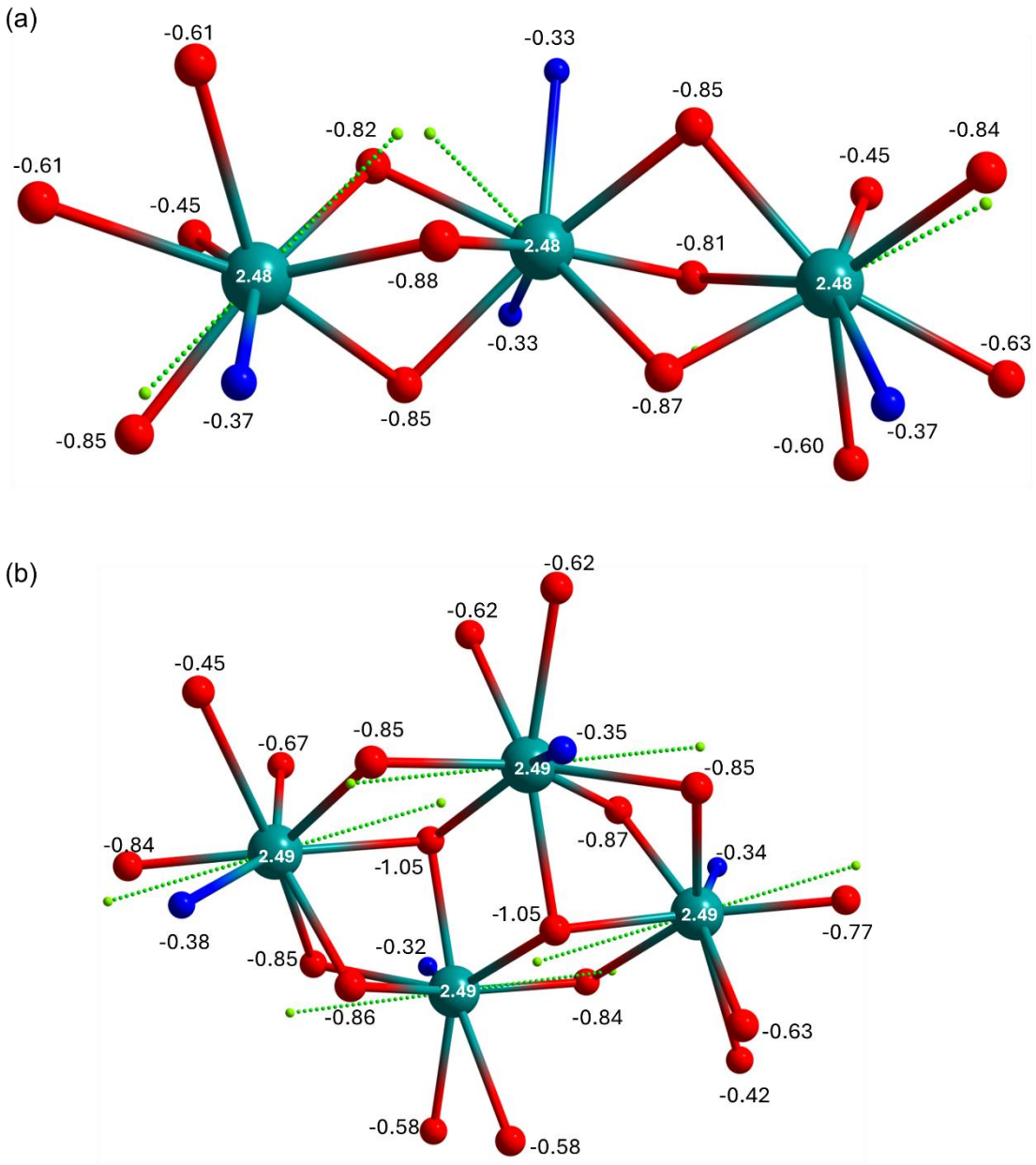

Fig. S17. CASSCF computed LoProp charges on the first coordinating atoms of (a)complex **1**; and (d) complex **2** respectively. (Color code: Dy - Teal; O -red; N-blue).

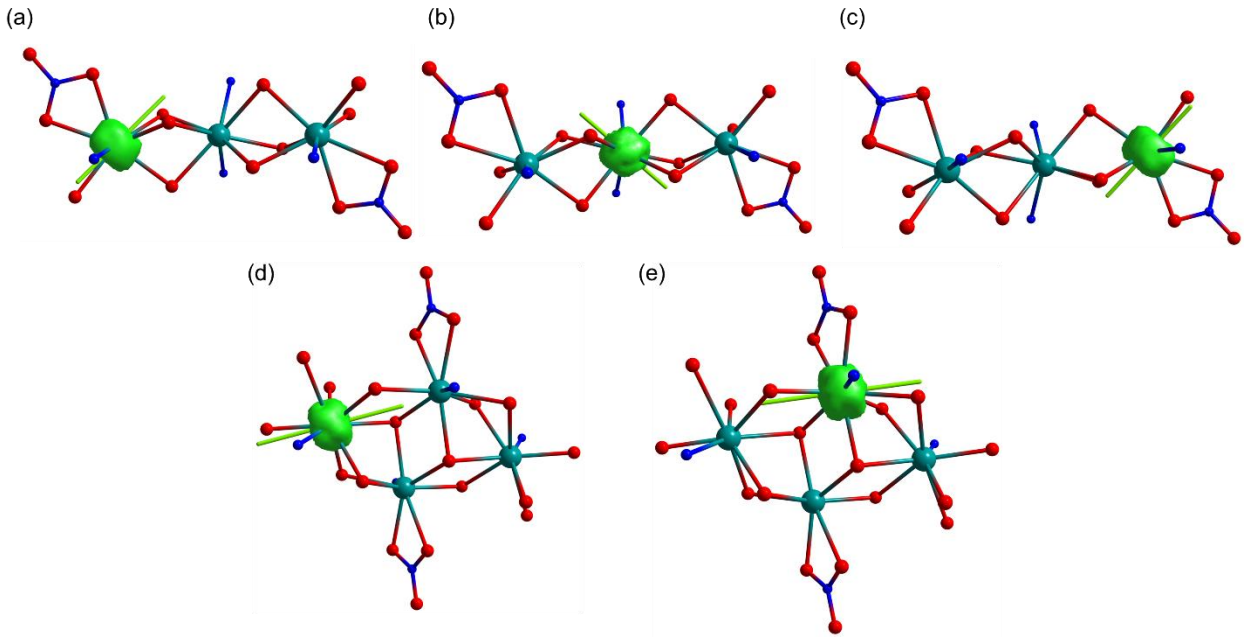

Fig. S18. CASSCF-computed beta-spin density for (a) **1**Dy@1, (b) **1**Dy@2, (c) **1**Dy@3, (d) **2**Dy@1/**2**Dy@1A and (e) **2**Dy@2/**2**Dy@2A. The CASSCF beta-spin density is plotted with an isosurface value of 0.009 e^{-}/bohr^3. Color code: teal(Dy), blue (N), red (O), gray (C), and white (H).

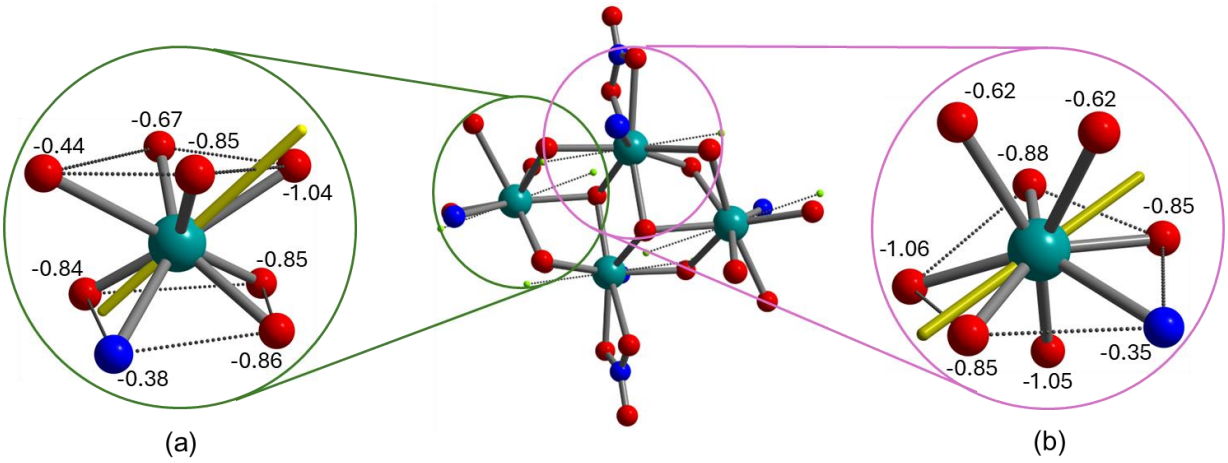

Fig. S19. (a) distorted square antiprismatic geometry around **2**Dy@1/1A and (b) distorted triangular dodecahedron around **2**Dy@2/2A of complex **2**.

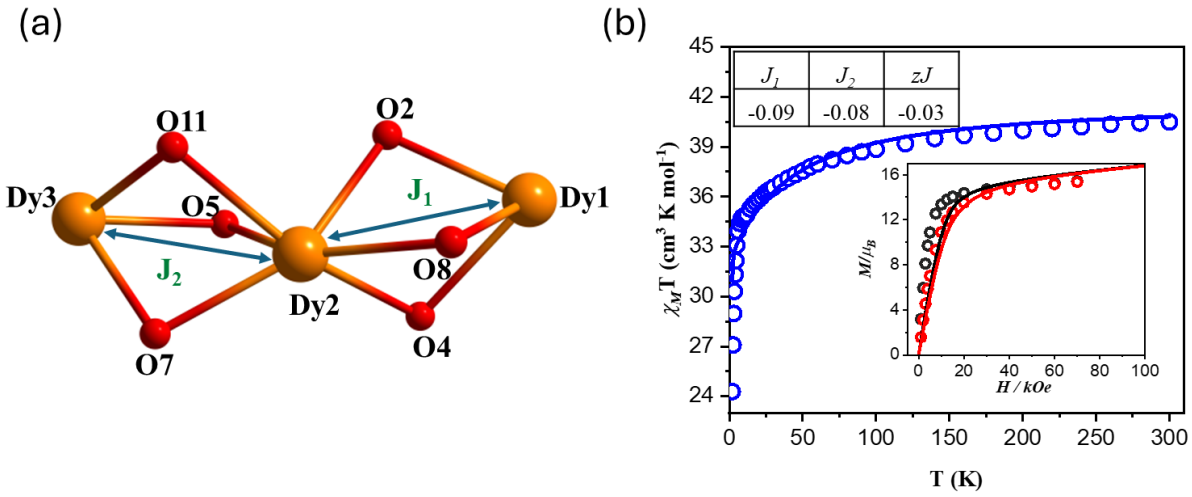

Fig. S20. (a) Model for magnetic exchange integrals and (b)thermal dependence of the $\chi_M T$ product in the 2-300 K temperature range for **1** (blue). In inset, field dependence of the magnetization at 2K (black) and 4K (red) in the 0-100 kOe field range. The corresponding solid lines represent the ab initio simulated magnetic data.The computed magnetic exchanges are given in Table 6. Here,we scaled down the simulated data by 3% to meet the experimental values.

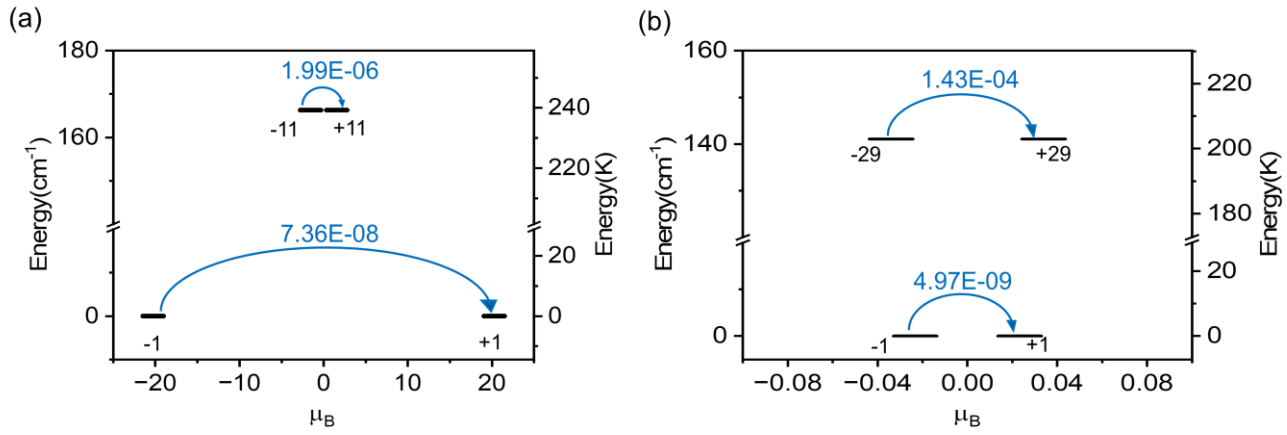

Fig. S21. POLY_ANISO computed *ab initio* blockade barrier for (a) $(Et_3NH)_2[Dy^{III}_3L_4(NO_3)_2]NO_3{\cdot}0.6Et_2O$ (**1**) and (b) $[Dy^{III}_4L_4(\mu_3\text{-}OH)_2(NO_3)_2(dmf)_2]$ (**2**).

Table S1. The values of selected bond angles in the coordination environment of the metal centers in Unit I of **1**.

O1−Dy1−N1	74.65(16)	N2−Dy2−N3	85.65(14)	N4−Dy3−O5	106.97(13)
O1−Dy1−O2	135.33(18)	N2−Dy2−O2	113.46(14)	N4−Dy3−O7	137.32(13)
O1−Dy1−O4	142.31(15)	N2−Dy2−O4	69.61(13)	N4−Dy3−O9	155.88(13)
O1−Dy1−O6	83.51(15)	N2−Dy2−O5	67.12(13)	N4−Dy3−O10	75.09(14)
O1−Dy1−O8	91.18(19)	N2−Dy2−O7	82.02(13)	N4−Dy3−O11	68.42(13)
O1−Dy1−O13	69.8(3)	N2−Dy2−O8	132.82(13)	N4−Dy3−O16	86.35(19)
O1−Dy1−O15	122.6(3)	N2−Dy2−O11	136.53(13)	N4−Dy3−O17	83.08(17)
O2−Dy1−O4	70.48(12)	O2−Dy2−O4	69.67(12)	O5−Dy3−O7	69.12(12)
O2−Dy1−O6	135.08(12)	O2−Dy2−O5	90.51(12)	O5−Dy3−O9	88.98(13)
O2−Dy1−O8	72.16(13)	O2−Dy2−O7	148.26(12)	O5−Dy3−O10	90.35(15)
O2−Dy1−O13	128.5(2)	O2−Dy2−O8	71.43(13)	O5−Dy3−O11	72.58(12)
O2−Dy1−O15	81.8(3)	O2−Dy2−O11	81.06(13)	O5−Dy3−O16	143.06(16)
O2−Dy1−N1	68.53(13)	O2−Dy2−N3	136.17(14)	O5−Dy3−O17	160.35(16)
O4−Dy1−O6	64.75(12)	O4−Dy2−O5	118.81(13)	O7−Dy3−O9	64.92(12)
O4−Dy1−O8	69.38(13)	O4−Dy2−O7	141.38(12)	O7−Dy3−O10	144.68(14)
O4−Dy1−O13	119.9(2)	O4−Dy2−O8	69.12(13)	O7−Dy3−O11	70.15(12)
O4−Dy1−O15	82.0(3)	O4−Dy2−O11	148.19(12)	O7−Dy3−O16	77.76(17)
O4−Dy1−N1	138.88(13)	O4−Dy2−N3	82.41(13)	O7−Dy3−O17	115.11(18)
O6−Dy1−O8	88.64(13)	O5−Dy2−O7	69.46(12)	O9−Dy3−O10	87.12(14)
O6−Dy1−O13	79.5(2)	O5−Dy2−O8	156.91(12)	O9−Dy3−O11	135.00(12)
O6−Dy1−O15	95.2(3)	O5−Dy2−O11	72.25(12)	O9−Dy3−O16	91.55(19)
O6−Dy1−N1	156.36(13)	O5−Dy2−N3	133.08(14)	O9−Dy3−O17	76.74(16)
O8−Dy1−O13	158.5(2)	O7−Dy2−O8	119.34(13)	O10−Dy3−O11	132.18(15)
O8−Dy1−O15	146.2(2)	O7−Dy2−O11	69.67(12)	O10−Dy3−O16	126.57(19)
O8−Dy1−N1	100.56(14)	O7−Dy2−N3	69.47(13)	O10−Dy3−O17	75.7(2)
O13−Dy1−O15	53.8(3)	O8−Dy2−O11	90.35(12)	O11−Dy3−O16	81.31(18)
O13−Dy1−N1	84.4(2)	O8−Dy2−N3	67.23(14)	O11−Dy3−O17	127.06(16)
O15−Dy1−N1	89.1(3)	O11−Dy2−N3	112.61(14)	O16−Dy3−O17	52.27(19)

Table S2. The values of selected bond distances in the coordination environment of the metal centers along with metal---metal distances in Unit II of **1**.

Dy4−N7	2.473(4)	Dy5−N8	2.535(4)	Dy6−N9	2.464(4)
Dy4−O19	2.188(4)	Dy5−N10	2.530(4)	Dy6−O23	2.395(4)
Dy4−O20	2.277(4)	Dy5−O20	2.319(3)	Dy6−O25	2.167(4)
Dy4−O22	2.325(3)	Dy5−O22	2.329(3)	Dy6−O26	2.312(3)
Dy4−O24	2.495(4)	Dy5−O23	2.374(4)	Dy6−O28	2.329(3)
Dy4−O29	2.400(4)	Dy5−O26	2.312(3)	Dy6−O30	2.505(4)
Dy4−O31	2.434(5)	Dy5−O28	2.343(3)	Dy6−O34	2.414(6)
Dy4−O32	2.424(6)	Dy5−O29	2.394(4)	Dy6−O35	2.437(6)
Dy4···Dy5	3.4857(4)	Dy5···Dy6	3.4885(4)		

Table S3. The values of selected bond distances and bond angles in the coordination environment of the metal centers along with metal---metal distances in Unit II of **1**.

N7−Dy4−O19	74.99(15)	N8−Dy5−N10	85.85(14)	N9−Dy6−O23	102.18(14)
N7−Dy4−O20	68.57(13)	N8−Dy5−O20	111.90(14)	N9−Dy6−O25	74.76(16)
N7−Dy4−O22	137.53(14)	N8−Dy5−O22	69.18(13)	N9−Dy6−O26	68.57(13)
N7−Dy4−O24	155.84(14)	N8−Dy5−O23	67.22(14)	N9−Dy6−O28	139.19(13)
N7−Dy4−O29	106.50(14)	N8−Dy5−O26	136.94(14)	N9−Dy6−O30	155.76(14)
N7−Dy4−O31	80.96(17)	N8−Dy5−O28	83.72(13)	N9−Dy6−O34	84.5(3)
N7−Dy4−O32	84.9(2)	N8−Dy5−O29	132.94(14)	N9−Dy6−O35	88.7(3)
O19−Dy4−O20	132.23(16)	N10−Dy5−O20	136.57(14)	O23−Dy6−O25	90.29(18)
O19−Dy4−O22	144.32(14)	N10−Dy5−O22	82.17(13)	O23−Dy6−O26	71.52(13)
O19−Dy4−O24	87.39(15)	N10−Dy5−O23	132.43(14)	O23−Dy6−O28	69.19(13)
O19−Dy4−O29	89.61(15)	N10−Dy5−O26	114.38(14)	O23−Dy6−O30	88.50(13)
O19−Dy4−O31	74.1(2)	N10−Dy5−O28	69.36(13)	O23−Dy6−O34	159.1(2)
O19−Dy4−O32	124.48(19)	N10−Dy5−O29	67.29(14)	O23−Dy6−O35	144.9(3)
O20−Dy4−O22	70.07(12)	O20−Dy5−O22	69.28(12)	O25−Dy6−O26	133.76(17)
O20−Dy4−O24	134.78(12)	O20−Dy5−O23	90.68(13)	O25−Dy6−O28	142.01(15)
O20−Dy4−O29	72.86(13)	O20−Dy5−O26	80.02(13)	O25−Dy6−O30	83.59(15)
O20−Dy4−O31	126.83(17)	O20−Dy5−O28	148.14(12)	O25−Dy6−O34	72.2(3)
O20−Dy4−O32	82.34(19)	O20−Dy5−O29	72.23(13)	O25−Dy6−O35	124.8(3)
O22−Dy4−O24	64.75(12)	O22−Dy5−O23	119.50(13)	O26−Dy6−O28	70.96(12)
O22−Dy4−O29	69.39(12)	O22−Dy5−O26	146.89(12)	O26−Dy6−O30	135.66(12)
O22−Dy4−O31	117.87(17)	O22−Dy5−O28	141.99(12)	O26−Dy6−O34	128.9(2)
O22−Dy4−O32	80.48(19)	O22−Dy5−O29	69.41(13)	O26−Dy6−O35	82.0(3)
O24−Dy4−O29	89.47(13)	O23−Dy5−O26	71.57(13)	O28−Dy6−O30	64.94(12)
O24−Dy4−O31	78.36(17)	O23−Dy5−O28	69.31(13)	O28−Dy6−O34	118.2(3)
O24−Dy4−O32	91.9(2)	O23−Dy5−O29	157.05(13)	O28−Dy6−O35	80.7(3)
O29−Dy4−O31	159.96(17)	O26−Dy5−O28	70.39(12)	O30−Dy6−O34	78.5(2)
O29−Dy4−O32	145.91(17)	O26−Dy5−O29	90.03(12)	O30−Dy6−O35	95.0(3)
O31−Dy4−O32	51.6(2)	O28−Dy5−O29	118.13(13)	O34−Dy6−O35	53.8(3)

Table S4. The values of selected bond angles in the coordination environment of the metal centers **2**.

N1−Dy1−O1	74.2(2)	N2−Dy2−O2A	135.8(2)
N1−Dy1−O2	66.6(2)	N2−Dy2−O4	73.3(2)
N1−Dy1−O4	78.88(19)	N2−Dy2−O5A	68.25(19)
N1−Dy1−O5	115.7(2)	N2−Dy2−O7	134.66(19)
N1−Dy1−O6	75.5(2)	N2−Dy2−O7A	86.60(19)
N1−Dy1−O7	133.29(19)	N2−Dy2−O9	74.3(2)
N1−Dy1−O8	148.9(2)	N2−Dy2−O10	119.5(2)
O1−Dy1−O2	116.9(2)	O2A−Dy2−O4	149.19(17)
O1−Dy1−O4	136.68(19)	O2A−Dy2−O5A	67.54(17)
O1−Dy1−O5	90.8(2)	O2A −Dy2−O7	78.91(17)
O1−Dy1−O6	77.6(2)	O2A −Dy2−O7A	78.67(17)
O1−Dy1−O7	151.04(18)	O2A −Dy2−O9	104.5(2)
O1−Dy1−O8	83.9(2)	O2A −Dy2−O10	87.5(2)
O2−Dy1−O4	80.99(17)	O4−Dy2−O5A	140.25(17)
O2−Dy1−O5	66.43(17)	O4−Dy2−O7	70.84(17)
O2−Dy1−O6	131.94(17)	O4−Dy2−O7A	96.49(18)
O2−Dy1−O7	76.10(17)	O4−Dy2−O9	92.4(2)
O2−Dy1−O8	144.35(18)	O4−Dy2−O10	83.0(2)
O4−Dy1−O5	131.75(18)	O5A−Dy2−O7	133.85(17)
O4−Dy1−O6	63.08(18)	O5A−Dy2−O7A	71.98(17)
O4−Dy1−O7	68.07(16)	O5A−Dy2−O9	86.7(2)
O4−Dy1−O8	103.95(19)	O5A−Dy2−O10	124.8(2)
O5−Dy1−O6	161.29(18)	O7−Dy2−O7A	71.04(19)
O5−Dy1−O7	70.13(17)	O7−Dy2−O9	133.3(2)
O5−Dy1−O8	85.93(19)	O7−Dy2−O10	82.5(2)
O6−Dy1−O7	114.16(17)	O7A−Dy2−O9	155.6(2)
O6−Dy1−O8	78.40(19)	O7A−Dy2−O10	151.99(19)
O7−Dy1−O8	73.44(18)	O9−Dy2−O10	51.7(2)

Table S5. The CASSCF/RASSI-SO/SINGLE_ANISO computed g-tensors,k_{QTM} (in μ_B), the angle of deviation from ground state g_{zz} orientation, relative energies and wave function decomposition analysis of eight low lying Kramers' doublets for **1**Dy@1 (Dy1 in Fig. 1) centre of complex **1**.

Energy (cm^{-1})	g_{xx}	g_{yy}	g_{zz}	k_{QTM}	θ (°)	m_J
0.0	0.004	0.004	19.922	1.35E-03	-	99.0% $\|\pm15/2\rangle$
168.3	0.003	0.007	17.180	1.72E-03	7.5	96.2% $\|\pm13/2\rangle$
359.3	0.465	0.601	14.138	1.78E-01	6.6	88.8% $\|\pm11/2\rangle$
502.6	2.095	2.392	11.579	8.11E-01	32.1	67.3% $\|\pm9/2\rangle$
580.0	3.655	5.294	12.095	2.77	83.7	34.1% $\|\pm7/2\rangle$ + 31.1% $\|\pm1/2\rangle$
641.1	0.070	1.210	16.595	5.29E-01	81.2	31.0% $\|\pm5/2\rangle$ + 23.8% $\|\pm7/2\rangle$
774.1	0.802	1.316	16.163	1.07	75.7	36.8% $\|\pm3/2\rangle$ + 21.3% $\|\pm1/2\rangle$
841.4	0.501	2.315	17.835	1.08	78.4	30.3% $\|\pm1/2\rangle$ + 27.1% $\|\pm5/2\rangle$

Table S6. RASSI-SO computed low-lying 21 spin-free sextet states and the spin-orbit coupled (Kramer doublets) for **1**Dy@1 center in complex **1**. All the values are reported here in cm^{-1}. The values in red colour are for the spin-free sextet states while the values in the blue colour are for the spin-orbit coupled states.

1Dy@1							
SPIN-FREE STATES		**SPIN-ORBIT COUPLED STATES**					
0.0	7754.6	0.0	3512.7	8152.5	10031.8	13840.9	38850.8
5.3	7839.7	168.3	3593.9	8247.2	10102.6	13868.3	38984.3
245.8	7846.8	359.3	3669.3	8341.8	10266.7	13923.5	39377.5
257.6	7960.2	502.6	3736.4	8464.7	11168.2	13966.2	40273.9
480.1	8042.6	580.0	5753.2	9760.4	11512.6	15259.4	40562.0
615.9	8071.9	641.1	5934.5	9811.6	11658.5	15290.0	40761.0
620.9	8088.9	774.1	6037.8	9847.4	12036.0	15326.8	41490.6
706.8	34526.8	841.4	6113.4	9890.1	12081.7	16284.6	41606.4
807.6	35345.1	3077.9	6201.6	9942.2	12107.8	16298.2	
872.9	35486.3	3293.1	6298.7	9961.5	12150.5	16894.8	
947.2		3414.7	8006.4	10016.4	12188.3	38786.9	

Table S7. The CASSCF/RASSI-SO/SINGLE_ANISO computed g-tensors, k_{QTM} (in μ_B), the angle of deviation from ground state g_{zz} orientation, relative energies and wave function decomposition analysis of eight low lying Kramers' doublets for **1**Dy@3 (Dy3 in Fig. 1) centre of complex **1**.

Energy (cm^{-1})	g_{xx}	g_{yy}	g_{zz}	k_{QTM}	θ (°)	m_J
0.0	0.005	0.006	19.963	1.79E-03	0.0	99.1% |±15/2⟩
163.6	0.020	0.032	17.249	8.85E-03	9.9	94.7% |±13/2⟩
342.0	0.740	0.954	14.011	2.83E-01	7.4	83.9% |±11/2⟩
473.1	2.117	3.014	11.489	9.46E-01	36.1	61.0% |±9/2⟩ + 15.0% |±3/2⟩
545.2	3.245	4.078	13.340	2.97	89.2	37.7% |±1/2⟩ + 30.9% |±7/2⟩
591.8	0.106	0.916	16.133	9.04E-01	78.5	35.0% |±5/2⟩ + 24.1% |±7/2⟩
736.0	1.678	5.731	10.721	1.97	76.6	46.7% |±3/2⟩ + 17.0% |±1/2⟩
783.3	12.896	7.615	0.924	1.94	22.1	30.0% |±1/2⟩ + 28.6% |±5/2⟩

Table S8. RASSI-SO computed low-lying 21 spin-free sextet states and the spin-orbit coupled (Kramer doublets) for **1**Dy@3 center in complex **1**. All the values are reported here in cm^{-1}. The values in red colour are for the spin-free sextet states while the values in the blue colour are for the spin-orbit coupled states.

1Dy@3							
SPIN-FREE STATES		**SPIN-ORBIT COUPLED STATES**					
0.0	7725.9	0.0	3483.5	8126.2	10003.0	13807.9	38843.9
6.6	7813.1	163.6	3554.7	8220.6	10068.3	13839.1	38971.8
225.0	7819.0	342.0	3631.5	8303.9	10225.2	13892.8	39324.4
248.0	7936.5	473.1	3677.8	8422.5	11155.6	13934.9	40249.4
445.2	8007.5	545.2	5744.8	9737.9	11479.9	15226.7	40526.9
582.2	8037.4	591.8	5914.4	9785.2	11607.3	15259.1	40700.8
598.8	8052.5	735.9	6011.7	9822.3	12007.3	15295.9	41451.8
641.7	34542.7	783.3	6082.2	9864.1	12055.5	16253.6	41559.5
769.7	35315.9	3074.4	6160.3	9911.5	12077.0	16265.8	
821.2	35408.6	3280.0	6253.0	9929.5	12118.7	16861.7	
907.7		3395.0	7994.3	9984.3	12154.1	38786.0	

Table S9. The CASSCF/RASSI-SO/SINGLE_ANISO computed g-tensors,k_{QTM} (in μ_B), the angle of deviation from ground state g_{zz} orientation, relative energies and wave function decomposition analysis of eight low lying Kramers' doublets for **1**Dy@2 (Dy2 in Fig. 1) centre of complex **1**.

Energy (cm^{-1})	g_{xx}	g_{yy}	g_{zz}	k_{QTM}	θ (°)	m_J
0.0	0.566	2.393	16.726	4.93E-01	0.0	52.2% |±15/2⟩+26.7% |±11/2⟩
19.7	0.383	0.511	16.777	2.21E-01	61.0	24.7% |±9/2⟩+16.3% |±7/2⟩
56.6	0.293	2.419	10.937	4.91E-01	26.3	33.8% |±13/2⟩+16.6% |±5/2⟩
93.6	0.972	2.291	17.861	8.44E-01	66.7	22.7% |±9/2⟩+22.5% |±7/2⟩
133.9	10.215	7.959	3.301	2.28	37.5	22.2% |±9/2⟩+22.0% |±7/2⟩
217.1	2.682	3.821	11.827	2.72	88.6	25.4% |3/2⟩+23.2% |±7/2⟩
257.0	1.464	4.605	13.683	2.67	84.6	45.0% |±1/2⟩+22.5% |±3/2⟩
320.9	0.144	0.835	17.737	1.72E-01	34.9	28.5% |±13/2⟩+23.9%|±15/2⟩

Table S10. RASSI-SO computed low-lying 21 spin-free sextet states and the spin-orbit coupled (Kramer doublets) for **1**Dy@2 center in complex **1**. All the values are reported here in cm^{-1}. The values in red colour are for the spin-free sextet states while the values in the blue colour are for the spin-orbit coupled states.

1Dy@2							
SPIN-FREE STATES		**SPIN-ORBIT COUPLED STATES**					
0.0	7549.1	0.0	3141.9	7859.9	9705.0	13479.9	38716.2
47.2	7596.3	19.7	3149.7	7878.6	9750.7	13520.1	38738.5
161.7	7663.8	56.6	3177.5	7947.7	9780.8	13569.7	38775.6
204.7	7729.1	93.6	3202.6	7982.6	11010.9	13585.4	40077.2
216.7	7731.2	133.9	5632.9	9492.2	11086.0	14896.5	40129.0
244.8	7761.9	217.1	5659.8	9508.1	11152.7	14931.1	40173.7
250.5	7805.2	257.0	5694.7	9526.3	11706.9	14961.7	41113.5
328.0	34791.6	320.9	5723.8	9546.3	11743.2	15924.7	41132.2
430.2	34888.4	3045.3	5763.3	9570.6	11758.6	15930.1	
499.5	34952.0	3057.7	5797.1	9601.4	11762.5	16522.8	
538.5		3105.7	7822.5	9620.6	11795.7	38691.6	

Table S11. SINGLE_ANISO computed crystal field parameters for **1** and **2**. The CF parameters were computed using the following equation, $\hat{H}_{CF} = \sum \sum_{k=-q}^{q} B_k^q \ O_k^q$ and here B_k^q and O_k^q are the crystal field parameters and Steven's operator, respectively.

k	q	B_k^q				
		1			2	
		1Dy@1	1Dy@2	1Dy@3	2Dy@1/1A	2Dy@2/2A
2	-2	2.40E+00	-3.88E-01	1.31E+00	1.46E+00	-3.10E+00
	-1	-6.29E+00	-2.24E+00	-6.86E+00	**4.97E+00**	4.50E+00
	0	**-1.03E+01**	2.16E-01	**-9.43E+00**	-4.81E+00	-2.96E+00
	1	-1.23E+00	-1.48E-02	-1.04E+00	3.64E+00	5.32E+00
	2	-6.06E-01	**2.71E+00**	-7.70E-01	-3.29E-02	**6.99E+00**
$\left\lvert\frac{Av.axial}{Av.\ non-axial}\right\rvert$		3.91E+00	1.61E-01	3.78E+00	1.90E+00	5.95E-01
4	-4	1.18E-01	-2.27E-03	1.00E-01	-4.83E-02	1.03E-01
	-3	-1.61E-01	**-4.70E-01**	-2.51E-01	**-3.66E-01**	1.05E-01
	-2	2.52E-02	4.39E-03	2.74E-02	-3.87E-02	-1.41E-01
	-1	1.09E-01	-8.72E-02	9.72E-02	1.89E-01	-1.23E-01
	0	-1.91E-02	4.28E-02	-2.21E-02	-2.83E-02	-1.65E-02
	1	-1.49E-02	-5.30E-03	-1.66E-02	1.12E-02	7.92E-02
	2	-7.22E-02	-3.38E-02	-8.33E-02	-9.11E-02	1.13E-01
	3	**-3.25E-01**	1.09E-02	**-2.85E-01**	1.67E-01	**2.75E-01**
	4	-1.59E-01	-4.97E-02	-1.67E-01	8.94E-02	-4.88E-02
6	-6	2.13E-03	6.44E-05	3.43E-03	-5.64E-03	4.74E-03
	-5	1.16E-02	**-2.73E-02**	**1.52E-02**	**8.53E-03**	**-8.98E-03**
	-4	-8.38E-04	-2.46E-04	-4.99E-04	-3.06E-04	1.14E-03
	-3	1.13E-02	-7.11E-03	1.05E-02	-3.61E-03	-6.05E-03
	-2	9.66E-05	-1.84E-04	1.97E-04	3.79E-03	1.60E-03
	-1	-8.61E-04	-2.94E-03	1.40E-04	-4.37E-03	3.22E-03
	0	6.10E-04	7.85E-04	5.80E-04	-1.73E-04	-2.80E-04
	1	3.73E-03	-4.68E-05	4.73E-03	-4.44E-03	4.89E-04
	2	4.80E-03	8.01E-04	5.23E-03	-2.32E-03	1.72E-03
	3	-1.45E-03	3.69E-04	-3.59E-03	4.60E-03	6.10E-03
	4	5.79E-04	-5.68E-04	-1.99E-05	4.06E-03	2.17E-03
	5	**1.17E-02**	2.29E-03	9.50E-03	7.34E-03	-5.05E-03
	6	3.23E-04	-5.11E-03	-6.62E-04	4.49E-04	1.49E-03

Table S12. The CASSCF/RASSI-SO/SINGLE_ANISO computed g-tensors, k_{QTM} (in μ_B), the angle of deviation from ground state g_{zz} orientation, relative energies and wave function decomposition analysis of eight low lying Kramers' doublets for **2**Dy@2/**2**Dy@2A (Dy2/Dy2A in Fig. 2) centre of complex **2**.

Energy (cm^{-1})	g_{xx}	g_{yy}	g_{zz}	k_{QTM}	θ (°)	m_J
0.0	0.134	0.397	18.424	8.86E-02	-	77.5% $\|\pm15/2\rangle$
69.2	1.439	2.727	13.391	7.25E-01	20.6	38.9% $\|\pm13/2\rangle$ + 37.2% $\|\pm9/2\rangle$
125.2	3.057	4.841	8.528	1.33	13.5	35.4% $\|\pm7/2\rangle$ + 17.7% $\|\pm3/2\rangle$
200.0	8.608	5.358	1.645	1.77	48.3	27.6% $\|\pm5/2\rangle$ + 19.3%$\|\pm11/2\rangle$
286.0	1.394	2.279	13.479	1.83	80.7	25.6% $\|\pm3/2\rangle$ + 15.7% $\|\pm9/2\rangle$
383.6	0.003	0.618	16.695	5.77E-01	96.9	42.6% $\|\pm1/2\rangle$ + 16.3% $\|\pm3/2\rangle$
424.9	0.318	0.502	18.669	2.56E-01	70.2	24.9% $\|\pm5/2\rangle$ + 24.6% $\|\pm7/2\rangle$
500.0	0.024	0.046	18.918	2.43E-02	66.5	17.2% $\|\pm7/2\rangle$ + 16.9% $\|\pm5/2\rangle$

Table S13. RASSI-SO computed low-lying 21 spin-free sextet states and the spin-orbit coupled (Kramer doublets) for **2**Dy@2/**2**Dy@2A center in complex **2**. All the values are reported here in cm^{-1}. The values in red colour are for the spin-free sextet states while the values in the blue colour are for the spin-orbit coupled states.

2Dy@2/2Dy@2A							
SPIN-FREE STATES		**SPIN-ORBIT COUPLED STATES**					
0.0	7594.8	0.0	3235.2	7946.3	9765.3	13594.5	38779.7
15.6	7617.5	69.2	3299.5	7993.3	9826.5	13618.6	38855.8
117.7	7684.2	125.2	3352.5	8044.2	9960.9	13676.6	38950.3
161.8	7733.7	200.0	3416.0	8167.5	11031.4	13703.9	40084.5
202.0	7812.3	285.9	5674.1	9553.1	11227.8	15005.6	40207.2
353.3	7824.3	383.6	5745.0	9624.7	11341.3	15040.9	40435.2
372.5	7856.2	424.9	5788.2	9662.0	11805.7	15073.3	41224.3
462.8	34678.0	500.0	5839.0	9678.9	11840.7	16032.6	41283.6
484.0	34842.0	3053.9	5889.2	9692.6	11859.2	16044.6	
586.0	35221.3	3118.7	5992.6	9708.4	11883.5	16635.6	
613.7		3171.8	7889.2	9723.7	11914.4	38679.2	

Table S14. The CASSCF/RASSI-SO/SINGLE_ANISO computed g-tensors, k_{QTM} (in μ_B), the angle of deviation from ground state g_{zz} orientation, relative energies and wave function decomposition analysis of eight low lying Kramers' doublets for **2**Dy@1/**2**Dy@1A (Dy1/Dy1A in Fig. 2) centre of complex **2**.

Energy (cm^{-1})	g_{xx}	g_{yy}	g_{zz}	k_{QTM}	θ (°)	m_J
0.0	0.018	0.035	19.742	8.71E-03	-	96.8% |±15/2⟩
161.7	0.454	0.653	16.694	1.88E-01	16.2	80.7% |±13/2⟩
261.5	4.198	5.017	10.873	1.78	45.3	34.3% |±11/2⟩ + 19.0% |±3/2⟩
322.5	3.363	5.414	7.758	1.78	59.5	27.1%|±1/2⟩ + 23.7%| ±11/2⟩
373.0	4.367	5.737	8.598	2.34	81.0	29.8% |±9/2⟩ + 22.3% |±1/2⟩
457.0	0.099	2.830	12.037	1.02	68.4	48.9% |±7/2⟩ + 21.8% |±5/2⟩
482.5	2.572	3.973	12.055	2.56	93.0	40.2% |±3/2⟩ + 20.1% |±5/2⟩
499.1	2.557	3.500	13.710	1.71	65.8	24.7% |±9/2⟩ + 24.0% |±1/2⟩

Table S15. RASSI-SO computed low-lying 21 spin-free sextet states and the spin-orbit coupled (Kramer doublets) for **2**Dy@1/**2**Dy@1A centers in complex **2**. All the values are reported here in cm^{-1}. The values in red colour are for the spin-free sextet states while the values in the blue colour are for the spin-orbit coupled states.

2Dy@1/2Dy@1A							
SPIN-FREE STATES		**SPIN-ORBIT COUPLED STATES**					
0.0	7638.5	0.0	3331.1	8014.0	9869.9	13665.5	38827.8
32.2	7703.2	161.7	3366.3	8076.2	9928.6	13702.1	38903.0
237.7	7784.7	261.5	3410.1	8132.0	10013.9	13747.9	39056.0
267.7	7845.9	322.5	3435.5	8215.7	11119.6	13777.3	40170.7
375.1	7856.3	373.0	5736.1	9658.8	11322.5	15081.0	40338.0
412.8	7877.4	457.0	5831.7	9669.9	11363.8	15111.4	40444.6
481.3	7918.2	482.5	5875.2	9711.5	11894.1	15150.5	41291.5
522.5	34698.3	499.1	5912.3	9730.8	11920.9	16107.1	41350.2
567.9	35086.0	3086.7	5970.6	9760.1	11929.9	16117.3	
594.7	35172.2	3235.0	6035.7	9783.4	11952.3	16709.1	
645.1		3289.2	7960.5	9805.9	11991.4	38785.3	

Table S16. A comparison of Dy−O−Dy bridge angle (°) and symbol for exchange interaction in complexes **1** and **2**.

Compound	**Bridge Angle**		**Symbol for exchange interaction in Fig. 23 and text**
Dy^{III}_3 Complex **1**	Dy1−O2−Dy2	98.72	-0.09
	Dy1−O4−Dy2	96.80	
	Dy1−O8−Dy2	94.02	
	Dy3−O11−Dy2	98.28	-0.08
	Dy3−O7−Dy2	97.02	
	Dy3−O5−Dy2	93.66	
Dy^{III}_4 Complex **2**	Dy2A−O2−Dy1	95.91	-0.09
	Dy2A−O5−Dy1	94.07	
	Dy2A−O7−Dy1	93.17	
	Dy2−O2A−Dy1A	95.91	-0.09
	Dy2−O5A−Dy1A	94.07	
	Dy2−O7A−Dy1A	93.17	
	Dy2−O4−Dy1	111.59	-0.14
	Dy2−O7−Dy1	109.26	
	Dy2A−O4A−Dy1A	111.59	-0.14
	Dy2A−O7A−Dy1A	109.26	
	Dy2−O7−Dy2A	108.94	-0.04
	Dy2−O7A−Dy2A	108.94	

Table S17. Energies of the low-lying non-Kramers' exchange doublets along with $g_{zz}$and k_{QTM} obtained from POLY_ANISO simulation of complex **1**.

Exchange doublets	Energy (cm^{-1})	g_{zz}	k_{QTM}
1	0.0	40.525	7.36E-08
2	2.5	19.468	6.02E-07
3	2.5	13.905	8.59E-07
4	5.0	39.969	1.55E-07
5	21.2	23.783	1.04E-07
6	22.2	22.178	1.60E-07
7	22.2	23.362	1.19E-07
8	23.2	51.690	6.39E-08

Table S18. Energies of the low-lying non-Kramers' exchange doublets along with $g_{zz}$and tunnelling gap obtained from POLY_ANISO simulation of complex **2**.

Exchange doublets	Energy/cm^{-1}	g_{zz}	Δ_{tunnel}
1	0.0	0.047	4.97E-09
2	1.7	39.495	1.58E-08
3	1.7	39.440	1.91E-08
4	2.8	75.920	3.9E-07
5	3.0	23.061	2.24E-06
6	3.0	23.050	9.65E-07
7	3.1	7.935	1.74E-06
8	3.3	0.049	8.26E-07

Table S19. Simplified pictorial presentation, formula and magnetic parameters of the Dy^{III}_4 defect dicubane compounds derived from 2-(2-hydroxy-3-ethoxybenzylideneamino)phenol, H_2L (OEt ligand) and 2-(2-hydroxy-3-methoxybenzylideneamino)phenol, H_2L' (OMe ligand).

Formula and Simplified Pictorial Presentation	U_{eff}	τ_0	**Coordination No. (Geometry)**	**Two-step relaxation process identified or mentioned**	**Ref.**
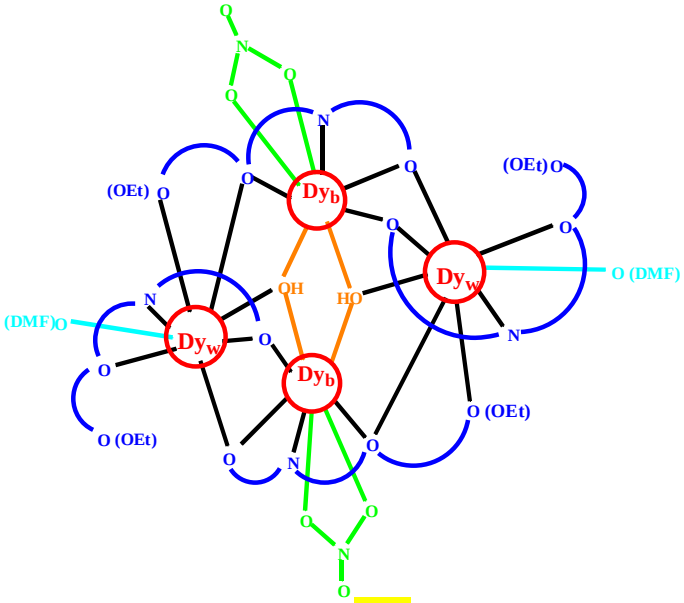 $[Dy^{III}_4L_4(\mu_3\text{-}OH)_2(NO_3)_2(dmf)_2]$ **(2)**	65.1 cm^{-1} under zero DC field	4.06×10^{-8} s	8 (TDD) for Dy_b 8 (SAPR) for Dy_w	Yes	This work

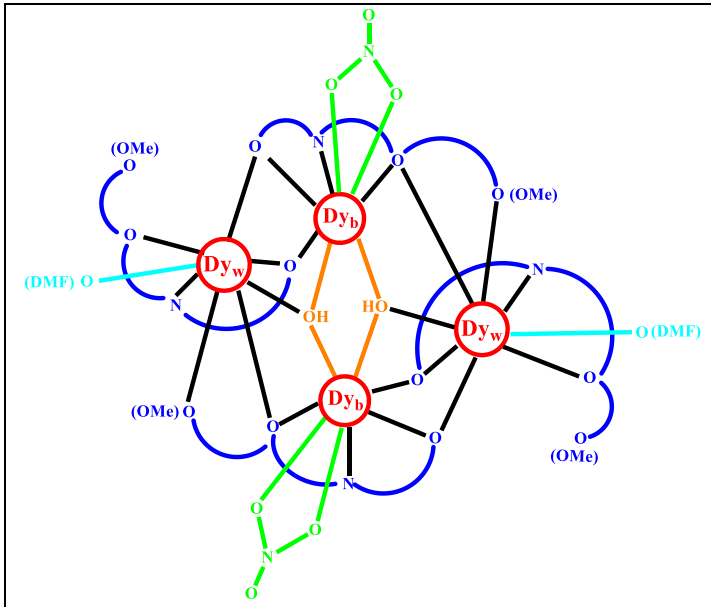 **[**$Dy^{III}_4L'_4(\mu_3\text{-}OH)_2(dmf)_2(NO_3)_2$] (**I**)	79.2 cm^{-1} under zero DC field	1.58×10^{-9} s	8 (BTPR) for Dy_b 8 (SAPR) for Dy_w	Yes	S1
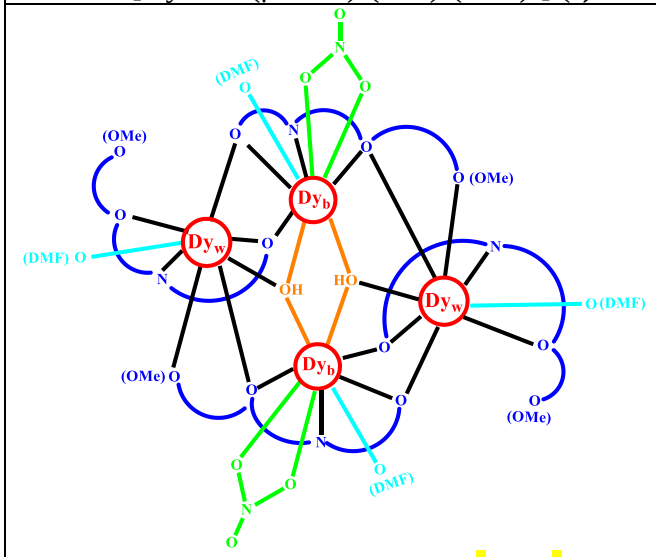 **[**$Dy^{III}_4L'_4(\mu_3\text{-}OH)_2(dmf)_4(NO_3)_2$]·2dmf·$H_2O$ (**II**)	Could not be evaluated as no maximum for χ_M'' up to 2 K	Could not be evaluated as no maximum for χ_M'' up to 2 K	9 (JTCTPR) for Dy_b 8 (SAPR) for Dy_w	Not Applicable	S2

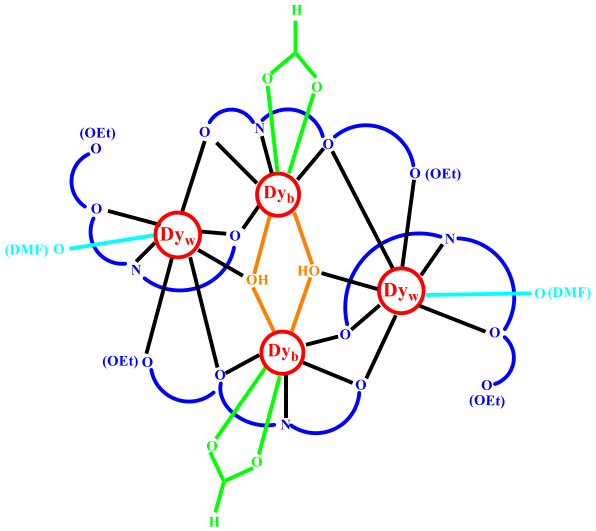 [$Dy^{III}_4L_4(\mu_3\text{-}OH)_2(formate)_2(dmf)_2$] **(III)**	49.0 cm^{-1}under zero DC field	1.76×10^{-7} s	8 (TDD) for Dy_b 8 (SAPR) for Dy_w	Yes	S3
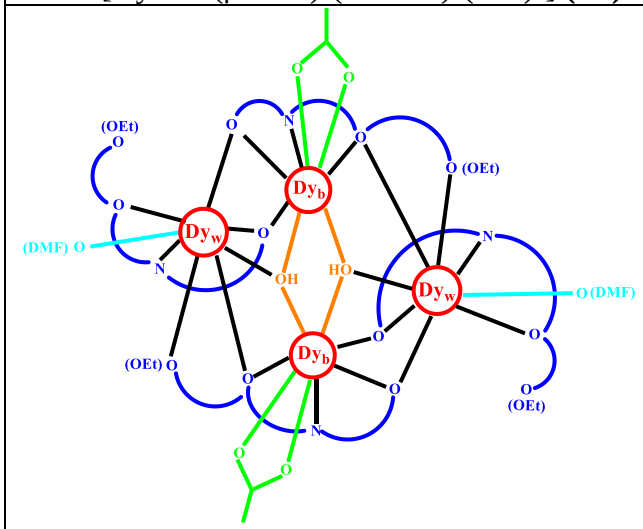 [$Dy^{III}_4L_4(\mu_3\text{-}OH)_2(acetate)_2(dmf)_2$] **(IV)**	30.3 cm^{-1}under zero DC field	1.51×10^{-8} s	8 (TDD) for Dy_b 8 (SAPR) for Dy_w	Yes	S3

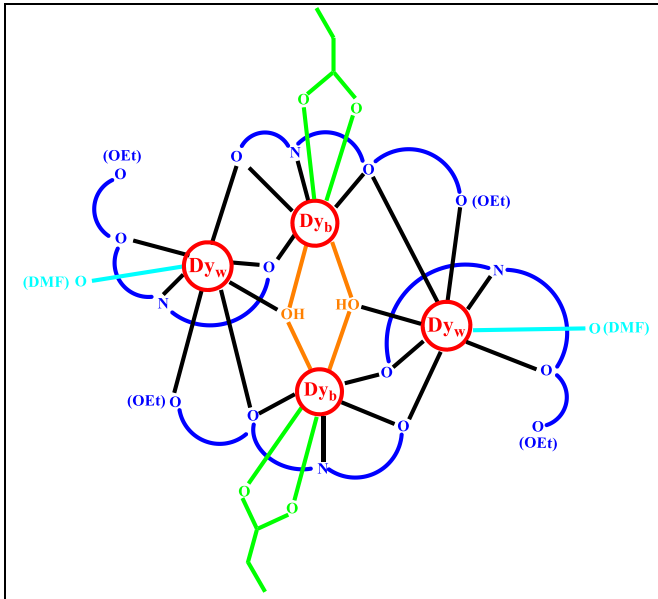 $[Dy^{III}_4L_4(\mu_3\text{-}OH)_2(propionate)_2(dmf)_2]$ **(V)**	23.4 cm^{-1}under zero DC field	9.64×10^{-7} s	8 (TDD) for Dy_b 8 (SAPR) for Dy_w	Yes	S3
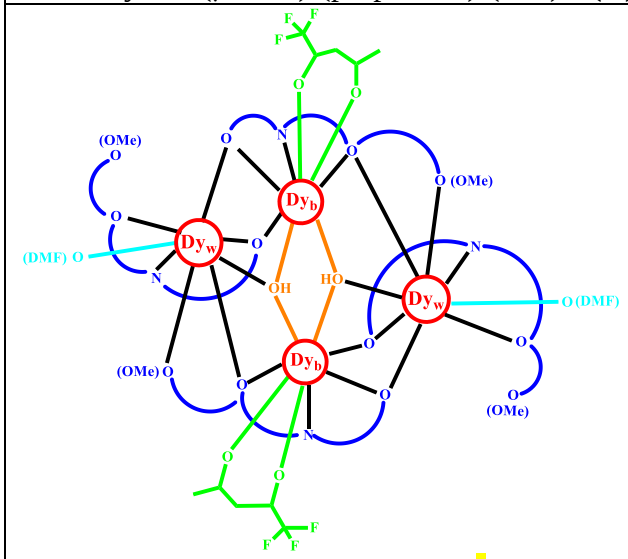 **[**$Dy^{III}_4L'_4(\mu_3\text{-}OH)_2(dmf)_2(tfaa)_2]\cdot 2CH_3CN$ (**VI**)	27.1 cm^{-1}under zero DC field	2.09×10^{-5} s	8 (BTPR) for Dy_b 8 (JBTPR) for Dy_w	Yes	S2

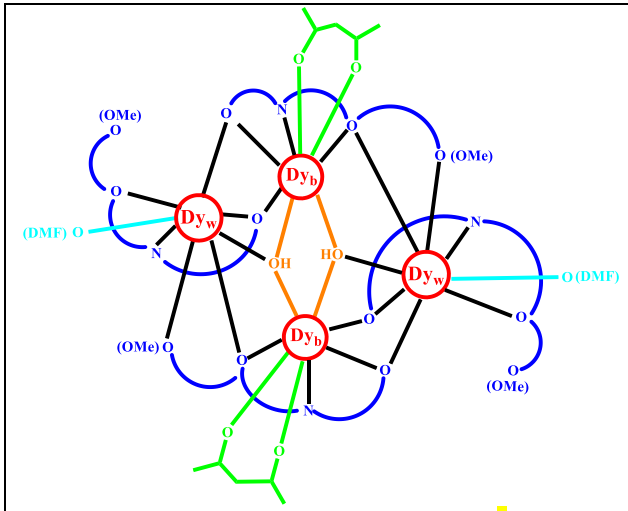 **[**$Dy^{III}_4L'_4(\mu_3\text{-}OH)_2(dmf)_2(acac)_2]\cdot 2dmf$ (**VII**)	65.3 cm^{-1}under zero DC field	9.62×10^{-7} s	8 (BTPR) for Dy_b 8 (JBTPR) for Dy_w	Yes	S2
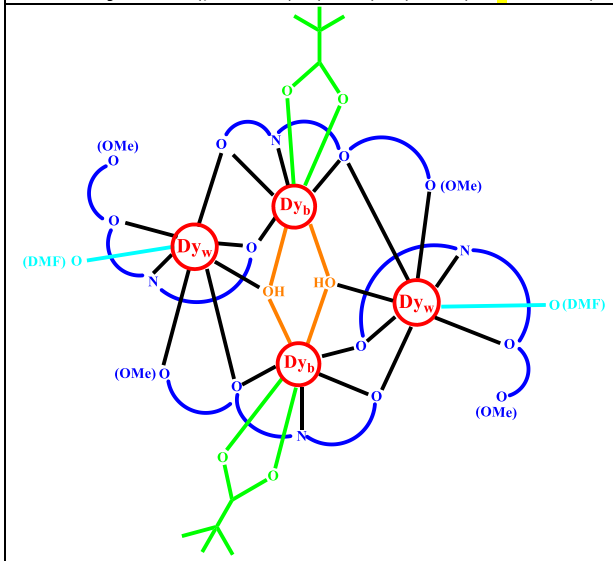 **[**$Dy^{III}_4L'_4(\mu_3\text{-}OH)_2(dmf)_2$ $(trimethylacetate)_2]\cdot 2CH_3CN$ (**VIII)**	38.9 cm^{-1} under zero DC field	2.66×10^{-8} s	8 (TDD) for Dy_b 8 (SAPR) for Dy_w	Yes	S4

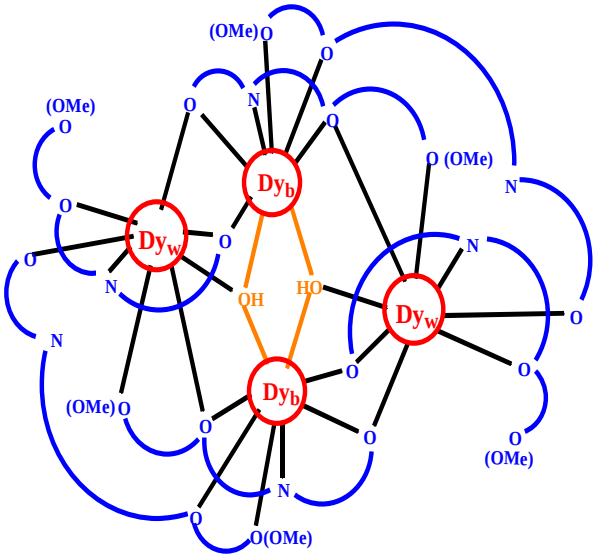 **[**$Dy^{III}_4L'_4(\mu_3\text{-}OH)_2(HL')_2]\cdot 2THF$ (**IX**)	2.6 cm^{-1} under zero DC field	4.8×10^{-5} s	8 (BTPR) for Dy_b 8 (SAPR) for Dy_w	No	S5
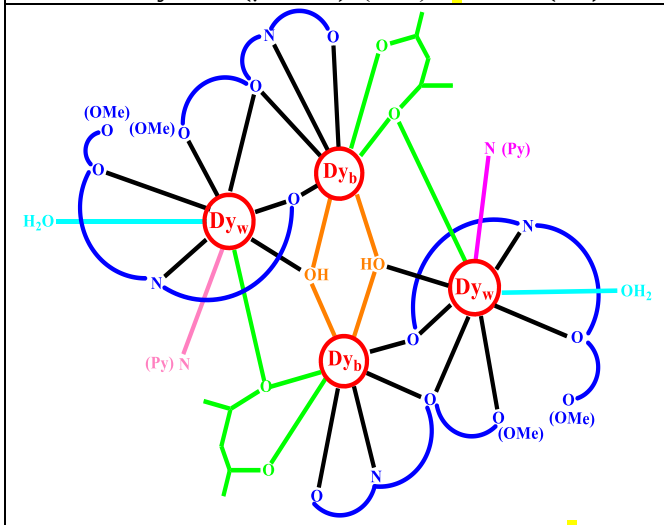 **[**$Dy^{III}_4L'_4(\mu_3\text{-}OH)_2(acac)_2(H_2O)_2(C_5H_5N)_2]\cdot 2THF$ (**X**)	25.7 cm^{-1} at 5 K 54.2 cm^{-1} at 15 Kunder zero DC field	5×10^{-7} s 7×10^{-7} s	8 (TDD) for Dy_b 9 (TCTPR) for Dy_w	Yes	S6

Table S20. Simplified pictorial presentation, formula and magnetic parameters of the non-linear tris((μ-phenoxido) bridged Dy^{III}_3 compounds derived from 2-(2-hydroxy-3-ethoxybenzylideneamino)phenol, H_2L (OEt ligand) and 8-hydroxyquinoline or its derivatives.

Formula and Simplified Pictorial Presentation	U_{eff}	τ_0	**Coordination No. (Geometry)**	**Two-step relaxation process identified or mentioned**	**Ref.**
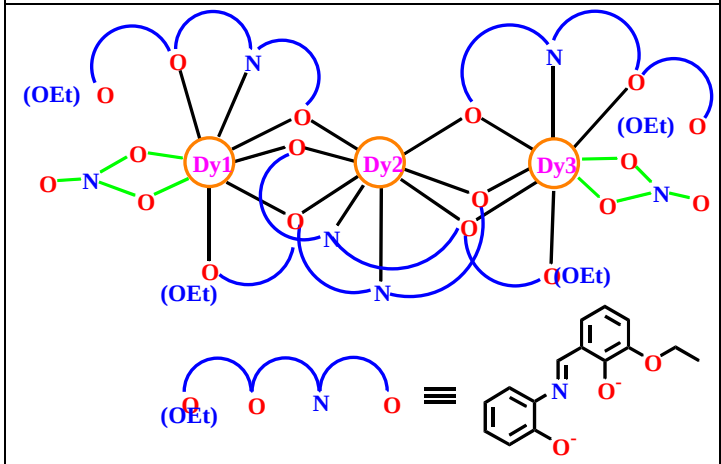 $(Et_3NH)_2[Dy^{III}_3L_4(NO_3)_2]NO_3{\cdot}0.6Et_2O$ **(1)**	32.3 cm^{-1} under 1000 Oe DC field	2.25×10^{-9} s	8 (TDD) for Dy1 and Dy3 of Unit I and Dy4 and Dy6 of Unit II 8 (SAPR) for Dy2 of Unit I and Dy5 of Unit II	Yes	This work

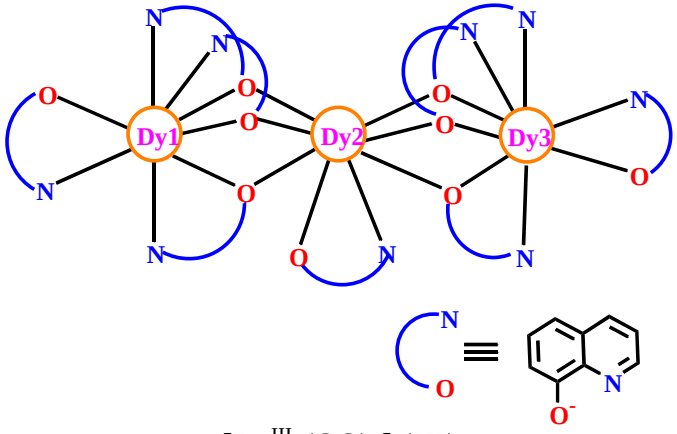 **[**$Dy^{III}_3(OQ)_9$] (**XI**) HOQ = 8-hydroxyquinoline	63.9 cm^{-1} for slow relaxation and 33.3 cm^{-1} for fast relaxation Under zero DC field	1.02 × 10^{-6} s for slow relaxation and 5.57 × 10^{-7} s for fast relaxation	8 (TDD) for Dy1 and Dy3 8 (SAPR) for Dy2	Yes	S7
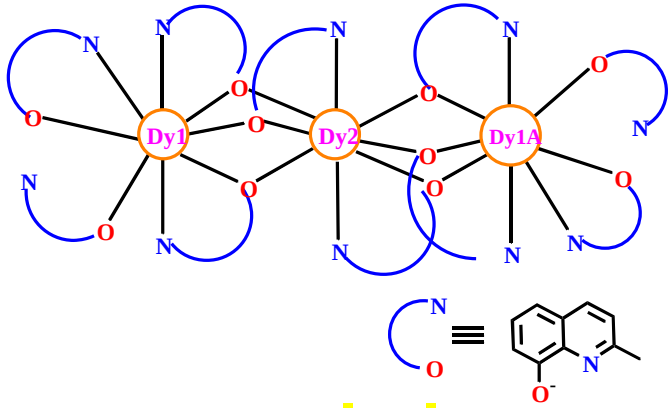 **[**$Dy^{III}_3(MQ)_9(HMQ)$]·$5H_2O$·3MeOH (**XII**) HMQ = 2-methyl-8-hydroxyquinoline	3.7 cm^{-1} under 2000 Oe DC field	9.6 × 10^{-6} s	8 (TDD) for Dy1and Dy1A 8 (SAPR) for Dy2	No	S8

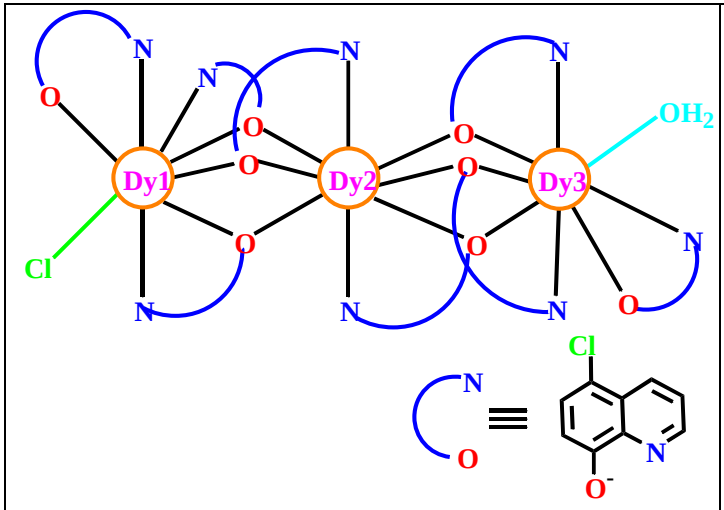 **[**$Dy^{III}_3(QCl)_8Cl(H_2O)$**](XIII)** HQCL = 5-chloro-8-hydroxyquinoline	50.0 cm^{-1}under 1700 Oe DC field	6.0×10^{-11} s	8 (TDD) for Dy1 and Dy3 8 (SAPR) for Dy2	No	S9
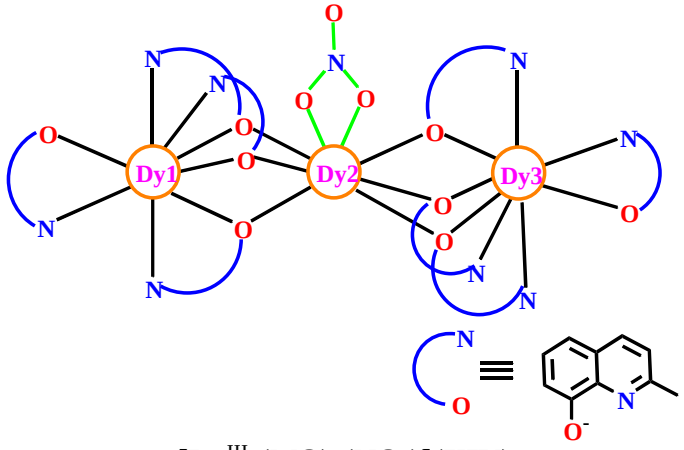 **[**$Dy^{III}_3(MQ)_8(NO_3)$**](XIV)** HMQ = 2-methyl-8-hydroxyquinoline	53.5 cm^{-1}under zero DC field and 169.6 cm^{-1} under 800 Oe DC field	1.22×10^{-6} s under zero DC field and 3.31×10^{-10} s under 800 Oe DC field	8 (BTPR) for Dy1 8 (SAPR) for Dy2 and Dy3	Yes	S10

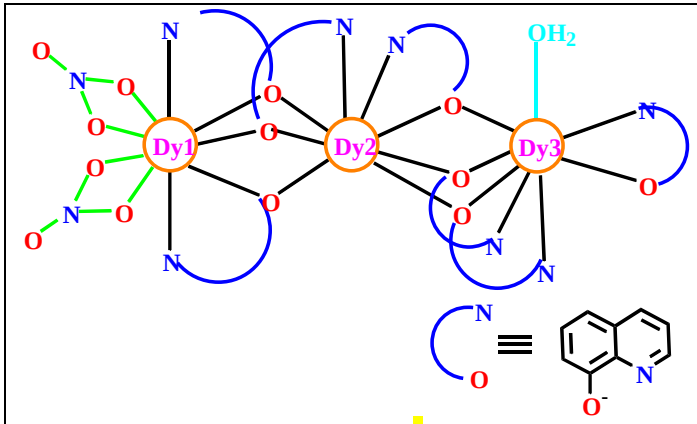 $Dy^{III}_3(hq)_7(NO_3)_2(H_2O)]\cdot 2.5MeCN$ **(XV)** hqH = 8-hydroxyquinoline	42.4 cm^{-1} under zero DC field	2.2×10^{-7} s	9 (TCTPR) for Dy1 8 (SAPR) for Dy2 and Dy3	No	S11

References

S1. K. Zhang, G.-P. Li, V. Montigaud, O. Cador, B. L. Guennic, J.-K. Tang and Y.-Y. Wang, *Dalton Trans*., 2019, **48**, 2135.

S2. K. Zhang, V. Montigaud, O. Cador, G.-P. Li, B. L. Guennic, J.-K. Tang and Y.-Y. Wang, *Inorg. Chem*., 2018, **57**, 8550.

S3. S. Mandal, A. Pramanik, S. Dey, L. M. Carrella, G. Rajaraman, E. Rentschler and S. Mohanta, *Dalton Trans*., 2022, **51**, 14753.

S4. K. Zhang, G.-P. Li, C. Zhang and Y.-Y. Wang, *J. Soild State Chem*., 2019, **273**, 11.

S5. K. C. Mondal, G. E. Kostakis, Y. Lan and A. K. Powell, *Polyhedron*, 2013, **66**, 268.

S6. A. K. Jami, J. Ali, S. Mondal, J. Homs-Esquius, E. C. Sañudo and V. Baskar, *Polyhedron*, 2018, **151**, 90.

S7. N. F. Chilton,G. B. Deacon,O. Gazukin,P. C. Junk, B. Kersting,S. K. Langley,B. Moubaraki,K. S. Murray,F. Schleife,M. Shome,D. R. Turnerand J. A. Walker, *Inorg. Chem*., 2014, **53**, 2528.

S8. N. F. Ghazali, W. Phonsri, K. S. Murray, P. C. Junk, G. B. Deacon and D. R. Turner, *Eur. J. Inorg.Chem*., 2019, 2549.

S9. N. F. Ghazali, K. R. Vignesh, W. Phonsri, K. S. Murray, P. C. Junk, G. B. Deacon and D. R. Turner, *Dalton Trans*., 2022, **51**, 18502.

S10. D.-P. Lv, J.-Y. Zheng, Q.-W. Li, J.-L. Liu, Y.-C. Chen, J.-H. Jia and M.-L. Tong,*Inorg. Chem. Front*., 2017, **4**, 1776.

S11. L. Batista, S. Paul, C. Molina-Jirón, J. A. Jaén, D. Fensker, O. Fuhr, M. Ruben, W. Wernsdorfer and E. Moreno-Pineda,*Dalton Trans*., 2024, **53**, 12927.